12-2016

Modeling, Optimizing and Testing Thermoelectric Generators for Liquid-to-Liquid Low Grade Waste Heat Recovery

Ali Eyddan Hamil
Western Michigan University, al_aiddan@yahoo.com

MODELING, OPTIMIZING AND TESTING THERMOELECTRIC GENERATORS FOR LIQUID-TO-LIQUID LOW GRADE WASTE HEAT RECOVERY

by

Ali Eyddan Hamil

A thesis submitted to the Graduate College
in partial fulfillment of the requirements
for the degree of Master of Science
Mechanical and Aerospace Engineering
Western Michigan University
December 2016

Thesis Committee:

HoSung Lee, Ph.D., Chair
Christopher Cho, Ph.D.
Bade Shrestha, Ph.D.

MODELING, OPTIMIZING AND TESTING THERMOELECTRIC GENERATORS FOR LIQUID-TO-LIQUID LOW GRADE WASTE HEAT RECOVERY

Ali Eyddan Hamil, M.S.E.

Western Michigan University, 2016

The use of thermoelectric generators (TEGs) for producing electricity from low grade waste heat is thought to be a great solution in the future to reduce the power generation cost because of their advantages of reliability and environmental friendliness. Therefore, the current project aims to study thermoelectric generators for low grade waste heat recovery. In this work, a single unit cell of liquid to liquid thermoelectric generator attached with heat exchangers (heat sinks) is modeled using an internal flow. Its optimum design is obtained based on heat sink optimization and the optimal design method. An analytical model of four unit cells system is simulated by combining the isolation method with the non-dimensional technique where the optimum parameters are obtained from the unit cell optimal design. Finally, to verify the accuracy of modeling the four unit cells system (whole system), an experiment is conducted. The experimental results are in reasonably good agreement with the analytical results.

ACKNOWLEDGMENTS

I would like to express my deepest appreciation to my advisor, Dr. HoSung Lee, for his inspiration and patience. My thesis could not have been accomplished without his guidance and encouragement. He always dedicates himself to teach his students, so I would be very thankful to him forever. I would also like to thank my thesis committee members, Dr. Cho and Dr. Shrestha for their valuable comments and corrections.

I take this opportunity to express my sincere thanks to my sponsor, the Higher Committee for the Education Development in Iraq (HCED), for providing funds to support my study.

I would like to thank my family, my mother, my wife, my kids, my brothers and sisters for all of their love and understanding. I could not have pursued my master degree without their support. My other relatives and friends deserve great thanks for their encouragement.

Ali Eyddan Hamil

TABLE OF CONTENTS

Table of Contents-Continued

CHAPTER

Table of Contents-Continued

CHAPTER

LIST OF TABLES

LIST OF FIGURES

List of Figures-Continued

List of Figures-Continued

CHAPTER I

INTRODUCTION

At the present time, there are obvious efforts to recover the waste energy and convert it into electricity using various sources of waste heat such as in power plants, automobiles, cooling system, etc. These efforts have been conducted toward reducing the electrical generation cost and decreasing the global air pollution. However, fossil fuels are still the main source for producing electricity [1]. Waste heat is classified based on temperature into high grade (high temperature) and low grade (low temperature). Many thermal processes produced an enormous amount of waste heat at low grade temperature of 150 ℃ or less which is in most cases released to the environment or discarded through the cooling system [2]. Globally, energy consumption is expected to rise by 71% where the carbon dioxide emissions may increase by more than 40% [3]. Recovering low grade waste heat is a challenging task so, researchers have been working toward finding alternative and reliable ways to reuse this energy. Also, the recovered energy will help to increase the efficiency and decrease the fuel cost of the thermal system [2].

Ebrahimi et al. (2014), proposed eight conventional technologies to recover low grade waste heat. These are plant or district heating, power plant co-location, absorption cooling, organic Rankine cycle, piezoelectrics, thermolectrics, desalination/clean water production and biomass co- location. The technology of thermoelctrics is thought to be an alternative solution for reusing the waste heat. However, thermoelctrics has low efficiency and is costly. Many studies have been conducted toward developing suitable material to

improve its performance for many applications such as in space, automobile, geothermal energy and other industrial heat generating process.

1.1 Thermoelectrics

Thermoelectrics is the method to directly convert the thermal energy into electricity or vice versa. Also, it can be defined as a solid-state mechanism that does not require maintenance or have no moving parts. Thermoelectric modules are classified into thermoelectric generators (TEGs) and thermoelectric coolers (TECs). There is a growing effort into developing the technology of thermoelectrics because of its advantages of reliability such as in space or for terrestrial uses. Thermoelectric generator (TEG) provides a great benefit to using for power generation such as for waste heat recovery in automobiles and in power plants or for renewable energy such solar thermoelectric generator (STEG) while thermoelectric cooler (TEC) is used for cooling and heating such as in medical and electronics devices. Basically, electricity generates in TEG due to the temperature difference between its hot and cold junctions. Naturally, heat flows from the hot to the cold which causes more electrons to move from the hot side to the cold side. Due to this movement of electrons, an electrical field flows against the temperature gradient as shown in Figure 1.1 [4]

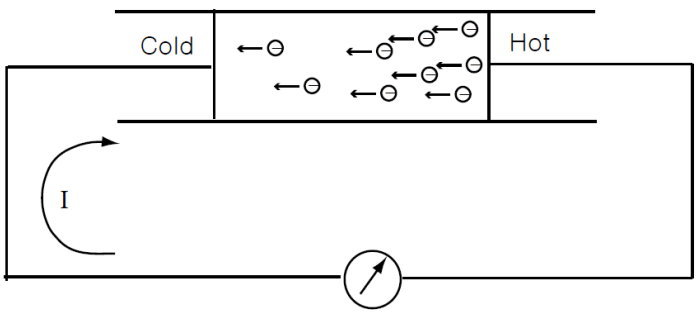

Figure 1.1 Movement of electrons in thermoelectric generator **[4]**

Thermoelectric modules consist of number of thermocouples connected electrically in series and thermally in parallel. Each couple has two semiconductor elements which are p-type and n-type. These couples are sandwiched between two ceramic plates that have low electrical conductivity and high thermal conductivity as shown in Figure 1.2.

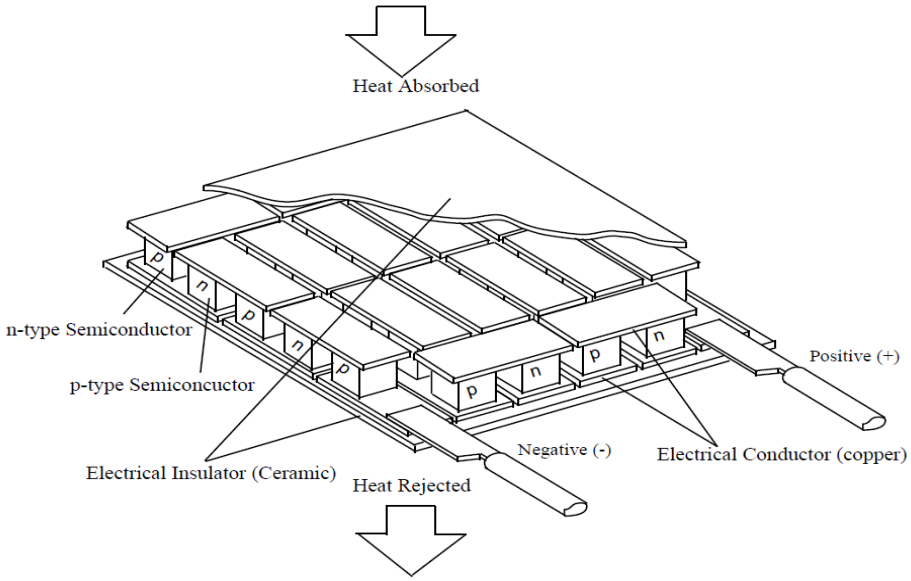

Figure 1.2 A typical thermoelectric module [4]

1.2 Thermolectric Effects

Thermometric effects are classified into Seebeck effect, Peltier effect and Thomson effect. In 1821, Thomas J. Seebeck found that if a circuit made from two dissimilar materials with different junction temperatures, an electrical potential could be produced. Later, Jean Peltier found that an electrical current would produce heating or cooling at the junction of two dissimilar materials. That was in 1834 and this effect is called Peltier effect. In 1854, William Thomson studied the relationship between the Seebeck and Peltier effects and found that heat is liberated or absorbed when current flows between two conductors

with existing temperature gradient. This is the third effect which is called Thomson effect. These three effects are described in the following [4].

1.2.1 Seebeck Effect

When a temperature difference is applied to two different materials, a potential difference, which is a voltage, will generate between the two sides of thermoelectric materials. On the another hand, it can be defined as the conversion of a temperature difference into an electric current [4] [5] & [6]. The voltage V is proportional to temperature differences in the following [4].

$$V = \alpha \Delta T \tag{1.1}$$

Where α is Seebeck coefficient,

1.2.2 Peltier Effect

It is an effect whereby heat must be continuously added or subtracted when current passes through a junction between two dissimilar conductors. The relationship between the heat and the current is proportional. It is defined by the following equation.

$$Q_{Peltier} = \pi_{AB} I \tag{1.2}$$

Where $Q_{Peltier}$ is the added or subtracted heat, π_{AB} the Peltier coefficient, I the current that passes across the junction [4], [5] & [6].

1.2.3 Thomson Effect

Thomson effect means that heat is absorbed or liberated when current passes between two different conductors with existing temperature gradient. Absorbed or liberated heat is proportional to the temperature difference and the passing current which it is defined in the following relationship.

$$Q_{Thomson} = \tau \Delta T I \tag{1.3}$$

1.3 The Figure of Merit

The figure of merit (Z) is a quantity used to determine the performance of thermoelectric (TE) devises. Its unit is $1/K$.

$$Z = \frac{\alpha^2}{\rho k} = \frac{\alpha^2 \sigma}{k} \tag{1.4}$$

Where α is the Seebeck coefficient in $\mu \frac{V}{K}$, ρ is the electrical resistivity in $\Omega\, cm$, k is the thermal conductivity in $\frac{W}{mK}$ and σ is the electrical conductivity where it is equal to $\frac{1}{\rho}$.

With most TE devises, the dimensionless figure of merit is used and defined as ZT where T represents the average temperature between the hot and cold junctions. Higher performance of TE devises is obtained when the value of ZT is bigger. To achieve a larger ZT value, the quantity of ($\alpha^2 \sigma$), called *power factor*, must be maximized and thermal conductivity which consists of electronic and lattice thermal conductivities must be minimized (k). Therefore, current researches are working to develop TE materials to have both higher Seebeck coefficient and electrical conductivity and lower thermal conductivity. The first generation of thermoelectric materials, developed between 1950-1960, have a ZT value up to one with conversion efficiency of 6%. Later, several experimental and theoretical studies were applied to further developing material with a range of a ZT of 1.3-1.7 at a high temperature, which is called the second generation of bulk thermoelectric materials. These materials, based on an approach that uses nanoscale materials and compositional in homogeneities to reduce the lattice thermal conductivities, can operate at conversion efficiencies of 11-15%. Recently, third generation of bulk thermometric

materials has been under development to create approaches to simultaneously improve Seebeck coefficient and reduce lattice thermal conductivity. These material shows high ZT value ranging from 1.8-2.2 with conversion efficiencies between 15-20% [4]& [7]. Figure 1.3 shows the dimensionless figure of merit for some nanocomposite thermoelectric materials.

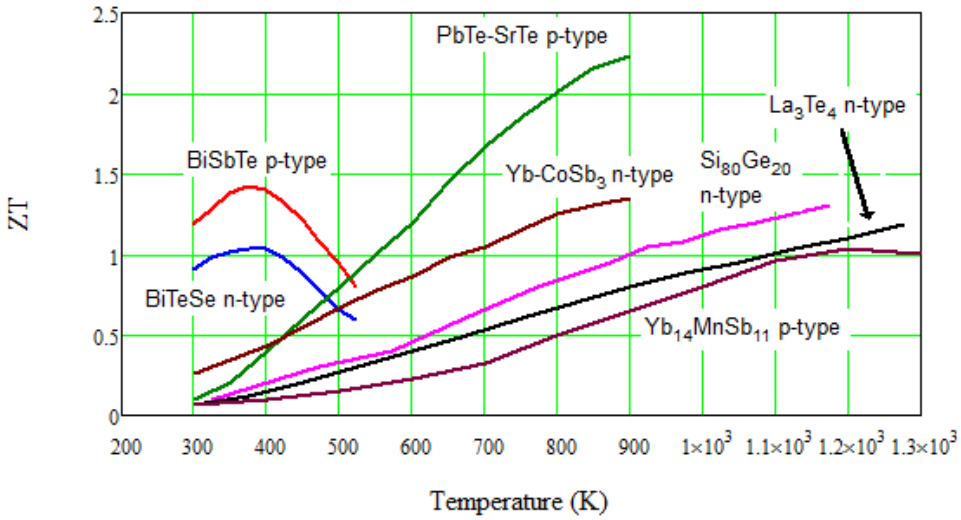

Figure 1.3 Dimensionless figure of merits for various nanocomposite materials **[4]**

1.4 Background of Thermoelectric Generators

Before dealing with modeling and optimizing of thermoelectric generators (TEGs) for low grade waste heat recovery, it is necessary to discuss the basic concepts of thermometrics.

1.4.1 Ideal Equations (Standard)

Based on the concepts of thermoelectric effects discussed in the previous section in this chapter, a circuit made from two dissimilar conductors can produce a voltage if one of the junctions is heated and the other is cooled. Therefore, heat is either absorbed or

liberated heat will consist of three parts, Joule heating, Peltier cooling and thermal conduction. All analyses are taken from references [4]& [6] with some explanation.

By considering thermoelectric generator module shown in figure 1.4 (a) consists of p-type and n-type thermocouples and assuming a steady state one-dimensional heat flow, no electrical and thermal contact resistances, convection and radiation are negligible and Seebeck coefficient is independent of temperature.

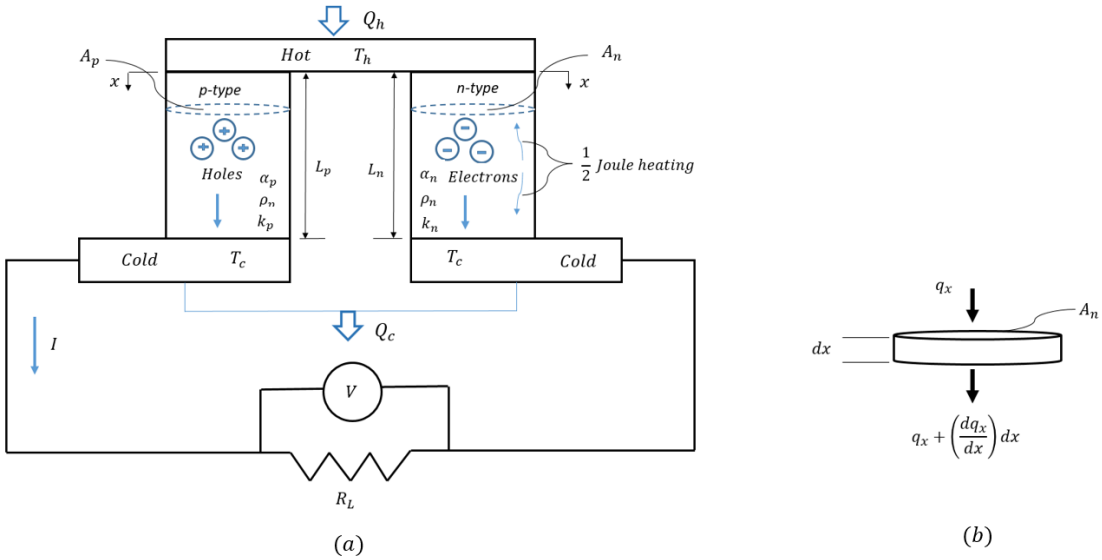

Figure 1.4 (a) p-type and n-type thermoelectric generator unit, (b) deffernetial element **[4]**

Based on the above assumption, the heat flows for n-type and p-type can be written as follows

$$q_p = \underbrace{\alpha_p T_h I}_{Peltier\ heat} + \underbrace{\left(-k_p A_p \frac{dT}{dx}\Big|_{x=0}\right)}_{Thermal\ conduction} \tag{1.5}$$

$$q_n = \alpha_n T_n I + \left(-k_n A_n \left.\frac{dT}{dx}\right|_{x=0}\right) \tag{1.6}$$

Where the first term in equations (1.5) & (1.6) is the Peltier heat and the second term is the thermal conduction.

By applying heat balance for differential element shown in figure 1.4 (b)

$$q_x - \underbrace{\left(q_x + \left(\frac{dq_x}{dx}\right)\right)}_{heat\ transfer\ at\ element\ surface} + \underbrace{\frac{I^2 \rho_p}{A_p}}_{Joul\ heating} = 0 \tag{1.7}$$

$$-\frac{d}{dx}\left(-k_p A_p \frac{dT}{dx}\right) + \frac{I^2 \rho_p}{A_p} = 0 \tag{1.8}$$

Using two boundary conditions ($T_{x=0} = T_h$ and $T_{x=L} = T_c$) so the temperature gradient can be written as following

$$\left.\frac{dT}{dx}\right|_{x=0} = \frac{I^2 \rho_p L}{2A^2 k} - \frac{T_h - T_c}{L} \tag{1.9}$$

Substituting equation (1.9) into equations (1.5) & (1.6)

$$q_p = \alpha_p T_h I - \frac{1}{2} I^2 \frac{\rho_p L_p}{A_p} + \frac{k_p A_p}{L_p}(T_h - T_c) \tag{1.10}$$

Similar way for n-type heat transfer,

$$q_n = -\alpha_n T_h I - \frac{1}{2} I^2 \frac{\rho_n L_n}{A_n} + \frac{k_n A_n}{L_n}(T_h - T_c) \tag{1.11}$$

The rate of heat absorbed at hot junction is

$$Q_h = q_p + q_n \tag{1.12}$$

Equation (1.12) becomes

$$Q_h = n\left[(\alpha_p - \alpha_n)T_h I - \frac{1}{2}I^2\left(\frac{\rho_p L_p}{A_p} + \frac{\rho_n L_n}{A_n}\right) + \left(\frac{k_p A_p}{L_p} + \frac{k_n A_n}{L_n}\right)(T_h - T_c)\right] \tag{1.13}$$

Furthermore,

$$\alpha = \alpha_p - \alpha_n \tag{1.14}$$

$$R = \frac{\rho_p L_p}{A_p} + \frac{\rho_n L_n}{A_n} \tag{1.15}$$

$$K = \frac{k_p A_p}{L_p} + \frac{k_n A_n}{L_n} \tag{1.16}$$

Where R is the is the electrical resistance and K is the thermal conductance

Finally, the heat rate at hot junction is given by

$$Q_h = n\left[\alpha T_h I - \frac{1}{2}I^2 R + K(T_h - T_c)\right] \tag{1.17}$$

Where n is the number of thermocouples and I is the generated current. By assuming thermocouples in n-type and p-type are same, equations (1.15) & (1.16) can be written as

$$R = \frac{\rho L}{A} \tag{1.18}$$

$$K = \frac{kA}{L} \tag{1.19}$$

Where $\rho = \rho_p + \rho_n$ and $k = k_p + k_n$

Similarly, the rate heat at cold junction is expressed as

$$Q_c = n\left[\alpha T_c I + \frac{1}{2}I^2 R + K(T_h - T_c)\right] \tag{1.20}$$

Equations (1.17) & (1.20) are called *ideal equations*. The power output (W_n) for the thermoelectric generator module is obtained by applying 1st law of thermodynamics.

$$W_n = Q_h - Q_c \tag{1.21}$$

Substituting equations (1.17) & (1.20) into equation (1.21)

$$V = \alpha \Delta T \tag{1.22}$$

Also, power output can be expressed in terms of circuit external load R_L

$$V = \alpha \Delta T \tag{1.23}$$

Which can also be expressed as

$$W_n = IV_n \tag{1.24}$$

Where V_n is the total voltage which can be given by

$$V_n = nIR_L = n[\alpha(T_h - T_c) - IR] \tag{1.25}$$

From the above equation, the electric current can be written in terms of internal resistance and external load

$$I = \frac{\alpha(T_h - T_c)}{R_L + R} \tag{1.26}$$

Also, the total voltage can be rewritten as

$$V_n = \frac{n\,\alpha(T_h - T_c)\frac{R_L}{R}}{\frac{R_L}{R} + 1} \tag{1.27}$$

Substituting equation (1.26) into equation (1.23)

$$W_n = \frac{n\,\alpha^2(T_h - T_c)^2}{R}\,\frac{\frac{R_L}{R}}{\left[1+\frac{R_L}{R}\right]^2} \tag{1.28}$$

The conversion or (thermal) efficiency is equal to the ratio between the power output to the input power or (absorbed heat) at hot junction

$$\eta_{th} = \frac{W_n}{Q_h} \tag{1.29}$$

Substituting equations (1.17) & (1.28) into the above equation

$$\eta_{th} = \frac{\left(1-\frac{T_c}{T_h}\right)\frac{R_L}{R}}{\left(1-\frac{R_L}{R}\right)-\frac{1}{2}\left(1-\frac{T_c}{T_h}\right)+\frac{1}{2Z\bar{T}}\left(1-\frac{R_L}{R}\right)^2\left(1+\frac{T_c}{T_h}\right)} \tag{1.30}$$

Where $\bar{T} = \frac{T_h+T_c}{1}$ is the average temperature and $\eta_c = \left(1-\frac{T_c}{T_h}\right)$ is the Carnot efficiency

The maximum electrical current is obtained when the external load (R_L) is equal to zero

$$I_{max} = \frac{\alpha(T_h - T_c)}{R} \tag{1.31}$$

The maximum voltage occurs when $I = 0$ (open circuit)

$$V_{max} = n\alpha(T_h - T_c) \tag{1.32}$$

Differentiating the power output in equation (1.28) with respect to resistance ratio ($\frac{R_L}{R}$) and setting it equal to zero, the maximum power output is obtained when the result gives $\frac{R_L}{R} = 1$

$$W_{max} = \frac{n\alpha^2(T_h - T_c)^2}{4R} \tag{1.33}$$

Similarly, the maximum conversion efficiency is obtained by differentiating equation (1.30) with respect to resistance ratio and setting it equal to zero. The result gives $\frac{R_L}{R} = \sqrt{1 + Z\bar{T}}$

$$\eta_{max} = \left(1 - \frac{T_c}{T_h}\right)\frac{\sqrt{1 + Z\bar{T}} - 1}{\sqrt{1 + Z\bar{T}} + \frac{T_c}{T_h}} \tag{1.34}$$

However, the maximum power efficiency, is the second type of efficiency that usually used with a commercial thermoelectric generator, is obtained when the power output is maximum. This is when $\frac{R_L}{R} = 1$

$$\eta_{mp} = \frac{\left(1 - \frac{T_c}{T_h}\right)}{2 - \frac{1}{2}\left(1 - \frac{T_c}{T_h}\right) + \frac{2}{Z\bar{T}}\left(1 + \frac{T_c}{T_h}\right)} \tag{1.35}$$

Now, there are five maximum parameters, $I_{max}, V_{max}, W_{max}, \eta_{max}$ and η_{mp} are essential to obtain a generalized curve for the performance of thermoelectric generator by dividing the actual parameters by the maximum parameters as shown in figure 1.5.

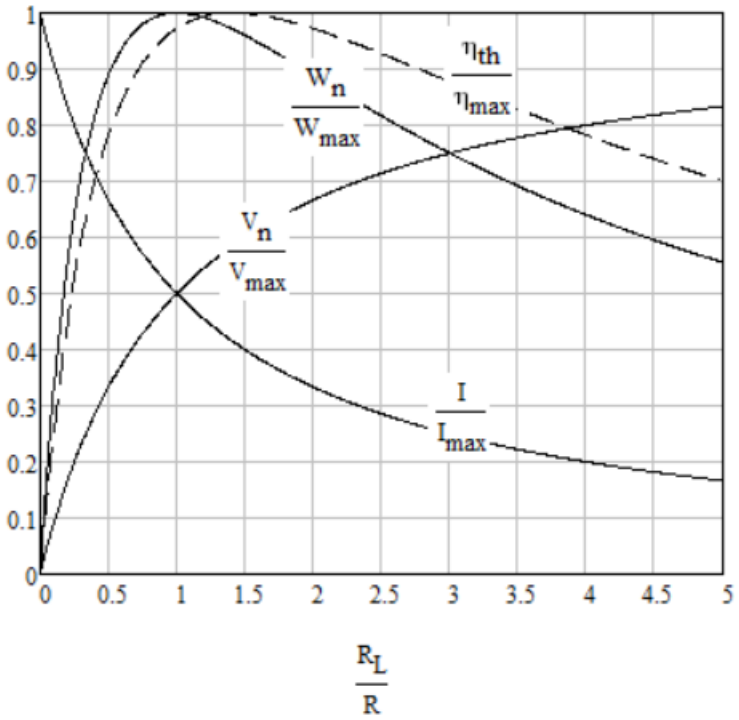

Figure 1.5 Normalized chart of TEG with assumptions of $\boldsymbol{Z\overline{T} = 1}$ and $\boldsymbol{\frac{T_c}{T_h} = 0.7}$ **[4]**

Figure 1.5 shows clearly that the maximum power output is when the ratio of external load resistance to the internal resistance of TEG are equal $\frac{R_L}{R} = 1$. Both maximum power output and maximum conversion efficiency seem to be close to each other and have the same curve trend but the maximum conversion efficiency happens when $\frac{R_L}{R} = 1.5$. Finally, all concepts related to TEG were described in detail in this chapter.

CHAPTER II

LITERATURE REVIEW AND OBJECTIVE

In order to carry out this study, some technical research papers have been referred to indicate what has been done by using thermoelectric generators for low grade waste heat recovery. All basic concepts of the thermoelectric generator were studied in the previous chapter, so the current chapter is to discuss some literature related to this study and sort its objectives.

2.1 Study of Related Work

Power generation from low temperature waste heat using thermoelectric generators has been investigated conceptually and experimentally since 1980. However, the first deep study in this area was conducted by Rowe et al. in 1997. They constructed a system that consists of 36 TEGs modules sandwiched between two heat exchangers (aluminum plate). The heat source was hot water with a temperature around 98℃ and for cooling they used cold water with a temperature around 20℃. Maximum power output was about 95 Watts when the system operated at hot side temperature of 97℃ and cold side temperature of 14℃. This study demonstrated that TEGs could be used to covert low temperature waste heat into electrical power although the conversion efficiency was low. They stated that the conversion efficiency is not an important consideration because the source of heat in such applications is free [8].

Another study, conducted by Crane et al in 2004, used a system of counter flow liquid to air for thermoelectric waste heat recovery. Their experimental model consisted of a single aluminum tube to flow hot water where three thermoelectric generator modules(TEGs) were in direct contact on each side of the tube and two cold air aluminum tubes around TEGs. Their purpose of this study was to verify the heat transfer through the TEGs and estimate the electrical and contact resistances. This study concludes that the power output of TEGs system is sensitive to fluid and air temperatures and it can be improved by maximizing the temperature difference across TEG and minimizing thermal resistance through using an optimized heat exchanger for waste heat recovery [9].

Yu et al presented a numerical study for power generation conversion using thermoelectrics technology. This work proposed a model used flat thermoelectric modules sandwiched between two parallel-plate heat exchangers as passages for hot water and cold water. One- dimensional heat flow and no heat losses between TEGs and the heat exchangers were the assumptions in this study. The results showed that the variation in temperature of fluids is linear even though two types of flow, parallel and counter, were employed. The variation in temperature difference was small for counter flow while there was a significant variation in parallel flow. The authors' goal of this study was to evaluate the performance of thermoelectric generator with parallel -plate heat exchanger under operation conditions [10].

Niu et al developed the numerical study, explained in the above, to experimentally validate a system using commercially thermoelectric generator modules made from Bismuth Telluride material for low grade waste heat recovery. 56 TEGs, each has 127 elements, were sandwiched between the cold and hot passages which were arranged in four

separate layers as multi-layer plate heat exchanger. Working fluids were a mixture of glycol/water for the hot and cold passages. Those TEGs were electrically connected in series and thermally in parallel. Two different configurations, parallel and counter flows, were considered in this work. The measurements were taken at range of operating temperatures, hot fluid between (50-150) ℃ and cold fluid (20-30) ℃, and the range fluid flow rate was between (0.2-0.6) $\frac{m^3}{h}$. Their results showed that at hot fluid temperature of 150 ℃, the measured power output was about 146.5 W while the predicted value was about 210 W. Authors concluded that the discrepancy between the prediction and measurement might be due to the heat losses which were not included in the numerical model. Also, another cause of the discrepancy is the thermoelectric properties are temperature dependent but they were assumed constant theoretically [11].

In 2010, Gou et al built an experimental model of liquid to air for power generation conversion. Their analysis was based on the fundamental of thermoelectricity and heat transfer irreversibility to predict the performance of thermoelectric generators for low grade waste heat recovery. The system consisted of a flow channel with a baffle in the center to circulate the hot water, 10 TECs arranged in two lines fixed on the flow channel and 10 heat sinks with axial fans for the cold side of the modules. Two cases, natural and forced convection, were employed in this work. Their measurement reasonably validated the analytical model in both cases. The results showed that expanding heat transfer capacity in the cold side would lead to a significant enhancement in power output while there is no much gain with improving heat transfer in the hot side [12].

A new study was published by Dai et al to verify the feasibility of thermoelectric generators for waste heat recovery based on liquid metal. Their method was to use liquid metal as a transporter for the heat that would be dissipated from waste heat into TE system due to its high thermal conductivity, low melting point, and high boiling point. Forty TE modules, liquid metal heating plate and two water cooling plates were the main parts of the power generation system. The modules were arranged on the two surfaces of the liquid metal plate where each of the water cooling plates was in contact with twenty modules. This study demonstrated that TE system using liquid metal is a feasible and flexible for waste heat recovery. The great advantages of using liquid metal are that it is efficient for heat transportation for long distance, and its ability of energy conservation [13].

Gou et al conducted a study in 2013 [14] using a similar configuration to what they published in 2010 [12]. They simulated and constructed a model of TE modules used liquid to air to harvest electricity from low temperature waste heat. Eighteen TECs are placed on each side of the hot water channel by nine modules for each side. The modules were cooled by six heat exchangers where the cooling air was forced by Two fans. Hot water temperature was between (50-90) ℃ and cold side was about 28.5℃. Hot water and air flow rates were about 2.76 m^3/h and 43.2 respectively. Maximum output was about 6.5 Watts at 90℃ with hot water flow rate of 2.76 m^3/h. The results showed that the analytical model was in good agreement with the results. The authors concluded that power output and conversion efficiency could be improved by enhancing the heat transfer in both hot and cold sides. However, power output generated by fluctuation of hot reservoir might be dangerous on the system design [14].

2.2 Summary of Literature Review

Some related works have been studied in the above section to evaluate the performance of TEGs for low grade waste heat recovery. Most of them were experimental works except one study was an analytical approach. Three different techniques, liquid to liquid, liquid to air and metal liquid to air have been used by the researchers to demonstrate the feasibility of thermometric generators to use in power generation from low temperature of waste heat. The conversion efficiency was too low but it can be considered as an insignificant parameter in some situations due to heat source is free [8]. Table 2.1 is a summary of literature review based on configuration.

Table 2.1 Summary of literature review based on configuration

Author(s)	Configuration	Type of work	Temperature	Number of TE modules	Comments
Rowe et al (1997)	Liquid to liquid	Experimental	Hot water =97℃ Cold water =14℃	36	Max. power =95W
Crane et al (2004)	Liquid to air	Experimental	Hot water =90℃ Cold air = 25℃	6	Max. power=0.54W
Niu et al (2009)	Liquid to liquid	Experimental	Hot fluid =150℃ Cold fluid =30℃	56	Max power =146.5W Max. efficiency =4.44% Power density =0.163 W/cm^2
Gou et al (2010)	Liquid to air	Experimental	Hot water =80℃ Cold air =24℃	10	Max. power = 0.85W Power density =0.0053 W/cm^2
Dai et al (2011)	Liquid metal to liquid	Experimental		40	Using liquid metal is highly feasible
Gou et al (2013)	Liquid to air	Experimental	Hot water =90℃ Cold air =28.5℃	18	Max. power = 6.5W Power density =0.0225 W/cm^2

2.3 Recent Optimal Studies

None of the above literature introduced an optimization technique to improve the performance of a thermoelectric generator itself for low grade waste heat recovery. The literature just focused on testing the commercial thermoelectric modules for low temperature waste heat. Lee [15] proposed a method for optimal design of thermoelectric devices, thermoelectric generator and cooler, using dimensionless analysis. This study considered a system consisted of thermoelectric device sandwiched between two heat sinks. Some dimensionless parameters were defined based on using the convection conductance in the denominators. For given fluids of the two heat sinks, either the optimal geometry ratio or the optimal number of elements of thermoelectric device and resistance ratio can be optimized. However, other parameters such as power output, conversion efficiency and can be maximized.

Lee's method has been demonstrated experimentally for thermoelectric coolers TECs by Alaa et al [16]. The authors simulated and validated an optimum design of automotive air to air thermoelectric air conditioner system. Their technique was to select a unit cell at the center to represent the entire system. The unit cell was analytically optimized and experimentally validated. The results were in good agreement with the analytical model. The powerful point of Lee's method of optimal design is it can be optimized two parameters simultaneously. For TEG, it can be optimized the resistance ratio and the dimensionless thermal conductance (geometry ratio or number of thermocouples) simultaneously. This method will be adopted in this study and it will discuss in detail in the next chapter.

2.4 Objective

After reviewing some related works that studied thermoelectric devises for recovering the energy from low temperature waste heat and understanding the principles of thermoelectric generator devises, the objective of this work is to study and develop the performance of thermoelectric generators for liquid to liquid low grade waste heat. The previous studies were focused on studying the feasibility of using thermoelectric generator for low grade where various configurations to recover the waste heat are presented. The current study focuses on modeling and optimizing the TEGs for liquid to liquid where two heat sinks are used for the hot and cold sides. The optimal design method [4] provides a simple technique based on non-dimensional parameters, so it can be applied to the liquid to liquid TEGs waste heat recovery. Also, an experiment is needed to verify the accuracy of modeling TEGs for low grade waste heat. Therefore, the following steps will be conducted to achieve this objective.

In chapter 3, the theories and methods of modeling the TEGs are discussed. Modeling of a single unit cell for liquid to liquid is described in the first part of this chapter. Then, the non-dimensional technique and heat sinks optimization are applied to the unit cell to obtain its optimal design. An analytical model of liquid to liquid four unit cells system is also modeled and optimized in this chapter.

Chapter 4 explains how the experiment is constructed and how the measurements are taken. This experiment is conducted to validate the accuracy of modeling four unit cells system presented in chapter 4.

Chapter 5 presents and discusses the results chapter 3 and 4. The results of modeling the unit cell before optimization is presented in the first part. Then, the results of the unit cell and the whole system after considering an optimized heat sink and applying the non-dimensional method are presented and compared with the previous results. A comparison between the experimental and analytical results of the four unit cells system is discussed in the last part of this chapter.

CHAPTER III

MODELING OF TEG FOR LOW GRADE WASTE HEAT RECOVEY

So far, the fundamental of thermoelectric generator and some recent studies have been discussed in chapter 1 & 2. The current chapter is to develop an analytical model of thermoelectric power generation for liquid-to-liquid low grade waste heat recovery. The model, shown in figure 3.1, mainly uses four thermoelectric generators sandwiched between two heat exchangers (heat sinks), one to flow the hot water and the other to flow the cold water. An internal flow is assumed in the analysis. To apply the optimal design method [15], the system is divided into equally unit cells where each unit cell consists of one TEG. Therefore, the optimization is applied just for a single unit cell. All analysis in this chapter are adopted from references [4], [5], and [15].

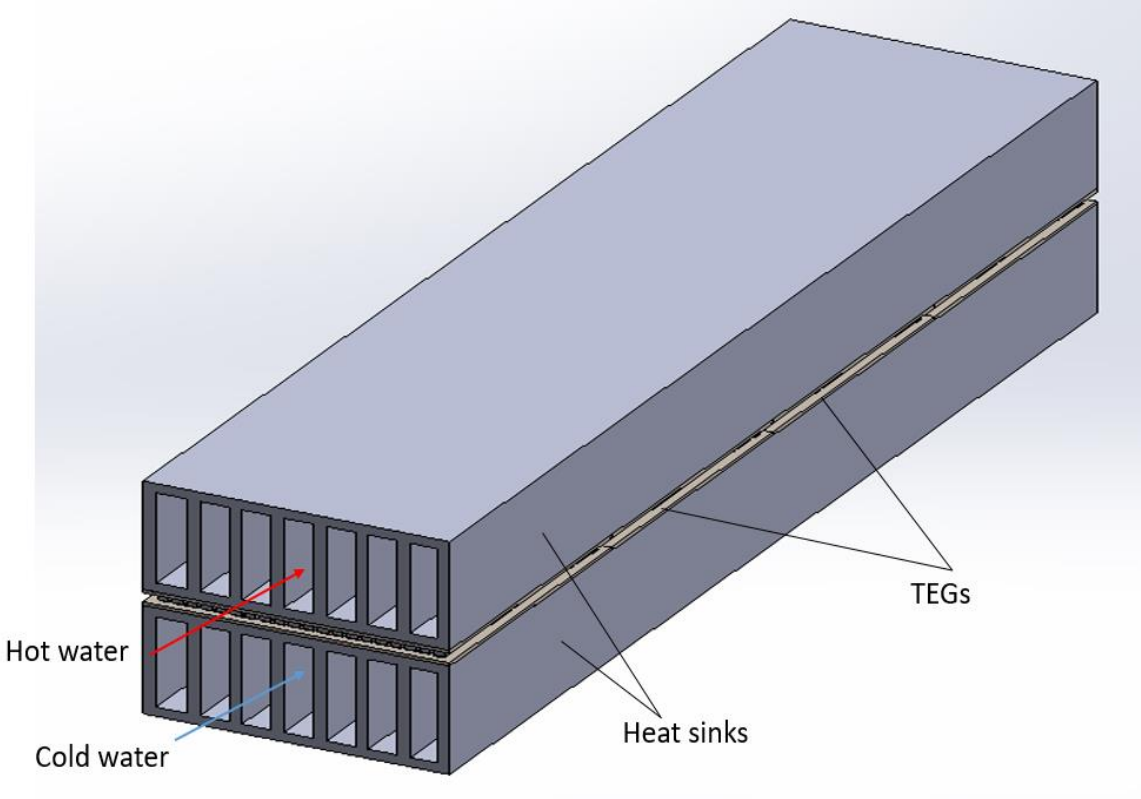

Figure 3.1 Schematic of TE system for low grade waste heat

3.1 Modeling of Single Unit Cell

In order to model the unit cell, a steady state one-dimension heat flow from the hot to the cold is assumed as shown in figure 3.2 (a). Through applying enthalpy flow across the heat sink, the absorbed heat (Q_h) by the heat sink is obtained as following.

$$Q_h = \dot{m}_h c_{p,h}(T_{\infty h,in} - T_{\infty h,out}) \quad (3.1)$$

Two assumptions are made. 1.) a uniform heat flow (linear temperature variation) through the heat sink and 2.) all heat $Q_h$must flow to the module, so the heat rate can be estimated between the average of the inlet and outlet water temperatures with hot junction temperature (T_h).

$$V = \alpha \Delta T Q_h = \eta_{s,h} h_h A_{s,h} \left(\frac{T_{\infty h,in} + T_{\infty h,out}}{2} - T_h \right) \tag{3.2}$$

Thermoelectric generator ideal equation is applied to the hot junction of the module.

$$Q_h = n \left[\alpha T_h I - \frac{1}{2} I^2 R + K(T_h - T_c) \right] \tag{3.3}$$

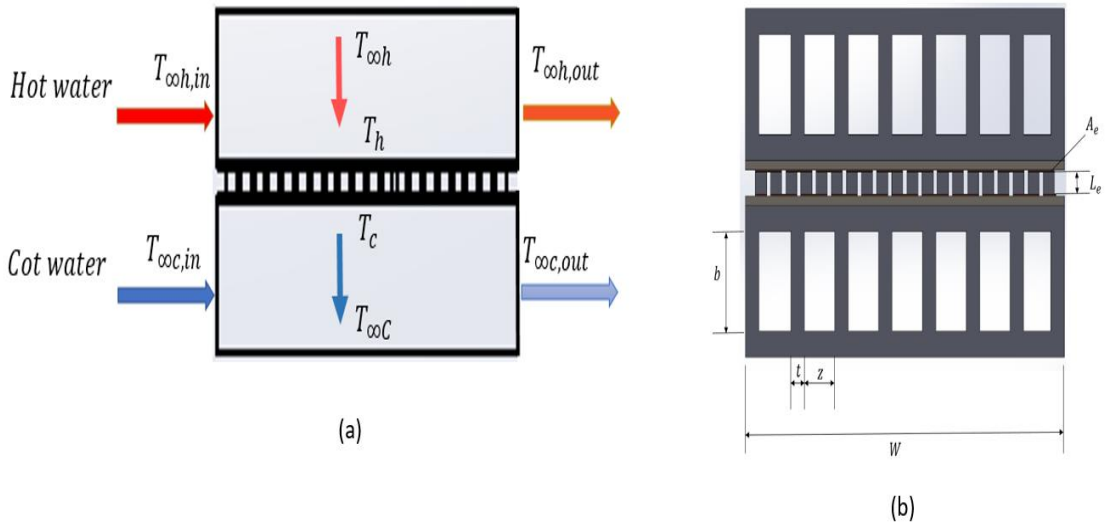

Figure 3.2 (a) Heat flow through the unit cell, (b) front view of the unit cell

Similar way for the cold side

$$Q_c = \dot{m}_c c_{p,c} (T_{\infty c,out} - T_{\infty c,in}) \tag{3.4}$$

$$Q_c = \eta_{s,c} h_c A_{s,c} \left(T_c - \left(\frac{T_{\infty c,in} + T_{\infty c,out}}{2} \right) \right) \tag{3.5}$$

$$Q_c = n \left[\alpha T_c I + \frac{1}{2} I^2 R + K(T_h - T_c) \right] \tag{3.6}$$

Where the internal resistance (R) and thermal conductance (K) are given by

$$R = \frac{\rho L_e}{A_e} \tag{3.7}$$

$$K = \frac{kA_e}{L_e} \tag{3.8}$$

The generated current is defined as

$$I = \frac{\alpha(T_h - T_c)}{\frac{R_L}{n} + R} \tag{3.9}$$

The power output is given by

$$W_n = Q_h - Q_c \tag{3.10}$$

Where Q_h andQ_c are the heat rate at hot and cold junctions, $\dot{m}_h$and $\dot{m}_c$ are the mass flow rate at hot and cold heat exchangers, $c_{p,h}$ and $c_{p,c}$ are the hot and cold specific heats, $\eta_{s,h}$ and $\eta_{s,c}$ are the hot and cold overall heat sinks efficiencies, h_h and h_c are the hot and cold heat transfer coefficients, $A_{s,h}$ and $A_{s,c}$ are the hot and the cold heat transfer areas of the heat sinks, $T_{\infty h,in}$, $T_{\infty h,out}$, $T_{\infty c,in}$ and $T_{\infty c,out}$ are the inlet and outlet temperatures of the hot and cold water, T_h and T_c are the hot and the cold junctions temperatures, α, ρ and k are the module properties, n is the number of module elements, A_e and L_e are cross section area and leg length of the module element and R_L is the external load.

3.2 Calculating of Convection Heat Transfer Coefficient, Overall Efficiency and Total Heat Transfer Area of the Heat Sinks

To calculate convection heat transfer coefficient, flow in duct is considered. Heat sinks of hot and cold sides are assumed to have same dimensions shown in figure 3.2 (b). The hydraulic diameter (D_h) is used for non-circular ducts. The Reyonlods number for flow in duct is given by

$$Re = \frac{VD_h}{\nu} \tag{3.11}$$

Where V is the velocity of the channel and ν is the kinematic viscosity. The flow is assumed as a turbulent ($Re_D > 2300$).

The hydraulic diameter is defined by

$$D_h = \frac{4A_c}{P_{wet}} \tag{3.12}$$

Where A_c and P_{wet} are the flow cross sectional area and the wetted perimeter.

The flow cross sectional area is given by

$$A_c = bz \tag{3.13}$$

And, the wetted perimeter is

$$P_{wet} = 2(b + z) \tag{3.14}$$

Where b and z are the profile length and the spacing of the heat sink respectively.

The Nusselt number for turbulent flow is

$$Nu_D = \frac{\left(\frac{f}{2}\right)(Re - 1000)Pr}{1 + 12.7\left(\frac{f}{2}\right)^{\frac{1}{2}}(Pr^{\frac{2}{3}} - 1)} \tag{3.15}$$

Where f is the friction factor and Pr is the Prandtal number.

The friction factor is expressed by

$$f = (1.58\ln(Re_D) - 3.28)^{-2} \tag{3.16}$$

The convection heat transfer coefficient is obtained by

$$h = \frac{Nu_D k_w}{D_h} \tag{3.17}$$

Where k_w is the thermal conductivity of the water.

The total heat transfer area of heat sink is defined by

$$A_s = n_f(2(L + t)b + Lz) \tag{3.18}$$

Where L and n_f are the length and the number of fins of heat sink respectively. In this work, the length and width of the module are assumed to be equal to the length and width of both heat sinks. For rectangular fins, the single fin efficiency is given by

$$\eta_f = \frac{\tanh(mb)}{mb} \tag{3.19}$$

Where

$$mb = \left[\frac{2h(t + L)}{k_m tL}\right]^{0.5} b \tag{3.20}$$

Where k_m is the thermal conductivity of heat sink material and b is the profile length. An aluminum heat sink is considered in this work.

Single fin surface area is defined as

$$A_f = 2(L + t)b \tag{3.21}$$

Finally, the overall heat sink efficiency is given by

$$\eta_s = 1 - n_f \frac{A_f}{A_t}(1 - \eta_f) \tag{3.22}$$

Based on the above equations, it can be estimated the convection conductance ($\eta_{s,h}h_hA_{s,h}$) and ($\eta_{s,c}h_cA_{s,c}$) where subscripts h and c denote the hot and cold quantities respectively.

3.3 Optimizing of Single Unit Cell Based on Dimensionless Parameters

As mentioned in chapter 2, the optimal method [15] provides the ability to optimize the power output and efficiency simultaneously with respect to both the geometry of element (geometric ratio or number of thermocouples) and the external load resistance. Based on using the convection conductance ($\eta_{s,c}h_cA_{s,c}$) of the cold side in denominators, some dimensionless parameters are introduced as in the following.

The dimensionless thermal conductance is defined by

$$N_k = \frac{n(G_e k)}{\eta_{s,c}h_cA_{s,c}} \tag{3.23}$$

Where $G_e = \frac{A_e}{L_e}$ is the geometric ratio

The dimensionless convection is defined by

$$N_h = \frac{\eta_{s,h}h_hA_{s,h}}{\eta_{s,c}h_cA_{s,c}} \tag{3.24}$$

The dimensionless electrical resistance is

$$R_r = \frac{R_L}{R} \tag{3.25}$$

The inlet temperatures of the hot and cold water ($T_{\infty h,in}$ and $T_{\infty c,in}$) shown in figure 3.2 (a) are given so, the dimensionless temperatures are defined by dividing on $T_{\infty c,in}$

$$T^*_{\infty h,in} = \frac{T_{\infty h,in}}{T_{\infty c,in}} \tag{3.26}$$

$$T^*_{\infty h,out} = \frac{T_{\infty h,out}}{T_{\infty c,in}} \tag{3.27}$$

$$T^*_{\infty c,out} = \frac{T_{\infty c,out}}{T_{\infty c,in}} \tag{3.28}$$

$$T^*_h = \frac{T_h}{T_{\infty c,in}} \tag{3.29}$$

$$T^*_c = \frac{T_c}{T_{\infty c,in}} \tag{3.30}$$

The dimensionless of heat rate at hot junction (Q^*_h), heat rate at cold junction (Q^*_c) and power output (W^*_n) are defined by

$$Q^*_h = \frac{Q_h}{\eta_{s,c} h_c A_{s,c} T_{\infty c,in}} \tag{3.31}$$

$$Q^*_c = \frac{Q_c}{\eta_{s,c} h_c A_{s,c} T_{\infty c,in}} \tag{3.32}$$

$$W^*_n = \frac{W_n}{\eta_{s,c} h_c A_{s,c} T_{\infty c,in}} \tag{3.33}$$

Equations (equation 3.1 to equation 3.6) are converted into four dimensionless equations as in the following

$$N_h \left[\frac{1}{2} T^*_{\infty h,in} + \frac{1}{2} T^*_{\infty h,out} - T^*_h\right] = N_k \left[\left(\frac{T^*_h - T^*_c}{(R_r + 1)}\right) T^*_h Z T_{\infty c,in} - \frac{(T^*_h - T^*_c)^2}{2(R_r + 1)^2} Z T_{\infty c,in} + (T^*_h - T^*_c)\right] \tag{3.34}$$

$$N_h \left[\frac{1}{2} T^*_{\infty h,in} + \frac{1}{2} T^*_{\infty h,out} - T^*_h\right] = \beta_1 \left[T^*_{\infty h,in} - T^*_{\infty h,out}\right] \tag{3.35}$$

$$N_h\left[T_c^* - \frac{1}{2}T_{\infty c,out}^* - \frac{1}{2}\right]$$

$$= N_k\left[\left(\frac{T_h^* - T_c^*}{(R_r+1)}\right)T_c^* ZT_{\infty c,in} + \frac{(T_h^* - T_c^*)^2}{2(R_r+1)^2}ZT_{\infty c,in} + (T_h^* - T_c^*)\right] \quad (3.36)$$

$$N_h\left[T_c^* - \frac{1}{2}T_{\infty c,out}^* - \frac{1}{2}\right] = \beta_2\left[T_{\infty c,out}^* - 1\right] \quad (3.37)$$

Where $ZT_{\infty c,in}$ is the dimensionless figure of merit. The expressions β_1 and β_2 are defined by

$$V = \alpha\Delta T \quad (3.38)$$

$$\beta_2 = \frac{\dot{m}_c c_{p,c}}{\eta_{s,c}h_c A_{s,c}} \quad (3.39)$$

The unknown dimensionless temperatures (T_h^*, T_c^*, $T_{\infty h,out}^*$ and $T_{\infty c,out}^*$) are placed as function of the five dimensionless parameters (N_k, R_r, N_h, $T_{\infty h,in}^*$ and $ZT_{\infty c,in}$) as in the below.

$$T_h^* = f(N_k, R_r, N_h, T_{\infty h,in}^*, ZT_{\infty c,in}) \quad (3.40)$$

$$T_c^* = f(N_k, R_r, N_h, T_{\infty h,in}^*, ZT_{\infty c,in}) \quad (3.41)$$

$$T_{\infty h,out}^* = f(N_k, R_r, N_h, T_{\infty h,in}^*, ZT_{\infty c,in}) \quad (3.42)$$

$$T_{\infty c,out}^* = f(N_k, R_r, N_h, T_{\infty h,in}^*, ZT_{\infty c,in}) \quad (3.43)$$

Therefore, the fourth unknown dimensionless temperatures can be estimated through solving equations (equation 3.34 to equation3.37). To apply the optimal method for the unit cell, the dimensionless convention (N_h), the dimensionless temperature of the hot,

water and the dimensionless figure of merit $ZT_{\infty c,in}$ are fixed. Then, the optimal N_k and R_r are obtained.

3.4 Effective Material Properties of TEGs

In order to calculate the performance of TEG using the ideal equations, shown in chapter 1, module material properties (α, ρ and k) must be known. However, using intrinsic material properties with the ideal equations lead to significant discrepancies with the provided performance curves of the commercial modules. This is because the thermal contact resistances, electrical contact resistances and the Thomson effects are assumed negligible in the ideal equations [4] [17].

Manufactures usually provide only the maximum parameters with the performance curves, so Lee developed a way to estimate the effective material properties of the commercial modules using the maximum parameters, maximum current (I_{max}), maximum voltage (V_{max}), maximum power output (W_{max}) and maximum power efficiency (η_{mp}). The obtained effective material properties include the Thomson effects, the radiation and convection heat losses and the thermal and electrical contact resistances [4]. The effective Seebeck coefficient (α^*), the effective electrical resistivity (ρ^*), the effective figure of merit (Z^*) and the effective thermal conductivity (k^*) are defined in the following.

$$\alpha^* = \frac{4W_{max}}{nI_{max}(T_h - T_c)} \tag{3.44}$$

$$\rho^* = \frac{4G_e W_{max}}{nI_{max}{}^2} \tag{3.45}$$

$$Z^* = \frac{\frac{2}{\overline{T}}\left(1+\frac{T_c}{T_h}\right)}{\eta_c\left(\frac{1}{\eta_{mp}}+\frac{1}{2}\right)-2} \tag{3.46}$$

$$k^* = \frac{\alpha^{*2}}{\rho^* Z^*} \tag{3.47}$$

Where η_c is the Carnot efficiency, and $\overline{T}$ is the average temperature.

3.5 Modeling of Four Unit Cells System

To simulate the four unit cells system, a thermal isolation method [18] is used where the whole system, schematically shown in figure 3.3, is assumed to consist of four isolated unit cells and each of them has one TEG module. This method allows us to determine the inlet and outlet water temperatures across each unit cell where a parallel flow is considered. The six heat balance equations (3.1, 3.2, 3.3, 3.4, 3.5 &3.6) are applied to each unit cell as follows.

$$Q_{hi} = n_i\left[\alpha^2 T_{hi}\frac{(T_{hi}-T_{ci})}{\left(\frac{R_{Li}}{n}+R\right)} - \frac{1}{2}\left(\frac{\alpha(T_{hi}-T_{ci})}{\left(\frac{R_{Li}}{n}+R\right)}\right)^2 R + K(T_{hi}-T_{ci})\right] \tag{3.48}$$

$$Q_{hi} = \eta_{s,h} h_h A_{s,h}\left(\frac{T_{\infty h,(i-1)i} + T_{\infty h,i(i+1)}}{2} - T_{hi}\right) \tag{3.49}$$

$$Q_{hi} = \dot{m}_h c_{p,h}(T_{\infty h,(i-1)i} - T_{\infty h,i(i+1)}) \tag{3.50}$$

$$Q_{ci} = n\left[\alpha^2 T_{ci}\frac{(T_{hi}-T_{ci})}{\left(\frac{R_{Li}}{n}+R\right)} + \frac{1}{2}\left(\frac{\alpha(T_{hi}-T_{ci})}{\left(\frac{R_{Li}}{n}+R\right)}\right)^2 R + K(T_{hi}-T_{ci})\right] \tag{3.51}$$

$$Q_{ci} = \eta_{s,c} h_c A_{s,c}\left(T_{ci} - \left(\frac{T_{\infty c,(i-1)i} + T_{\infty c,i(i+1)}}{2}\right)\right) \tag{3.52}$$

Where the subscript i represents the unit cell number ($i = 1\ to\ 4$), $T_{\infty h,01}$ and $T_{\infty c,01}$ are the hot and cold water inlet temperatures ($T_{\infty h,in}$ & $T_{\infty c,in}$) and $T_{\infty h,45}$ and $T_{\infty c,45}$ are the hot and cold water outlet temperatures ($T_{\infty h,out}$ & $T_{\infty c,out}$).

The total of hot junction rate, cold junction rate, power output and conversion efficiency are given by

$$Q_{h,total} = Q_{h1} + Q_{h2} + Q_{h3} + Q_{h4} \tag{3.53}$$

$$Q_{c,total} = Q_{c1} + Q_{c2} + Q_{c3} + Q_{c4} \tag{3.54}$$

$$W_{n,total} = Q_{h,total} - Q_{h,total} \tag{3.55}$$

$$\eta_{th,total} = \frac{W_{n,total}}{Q_{h,total}} \tag{3.56}$$

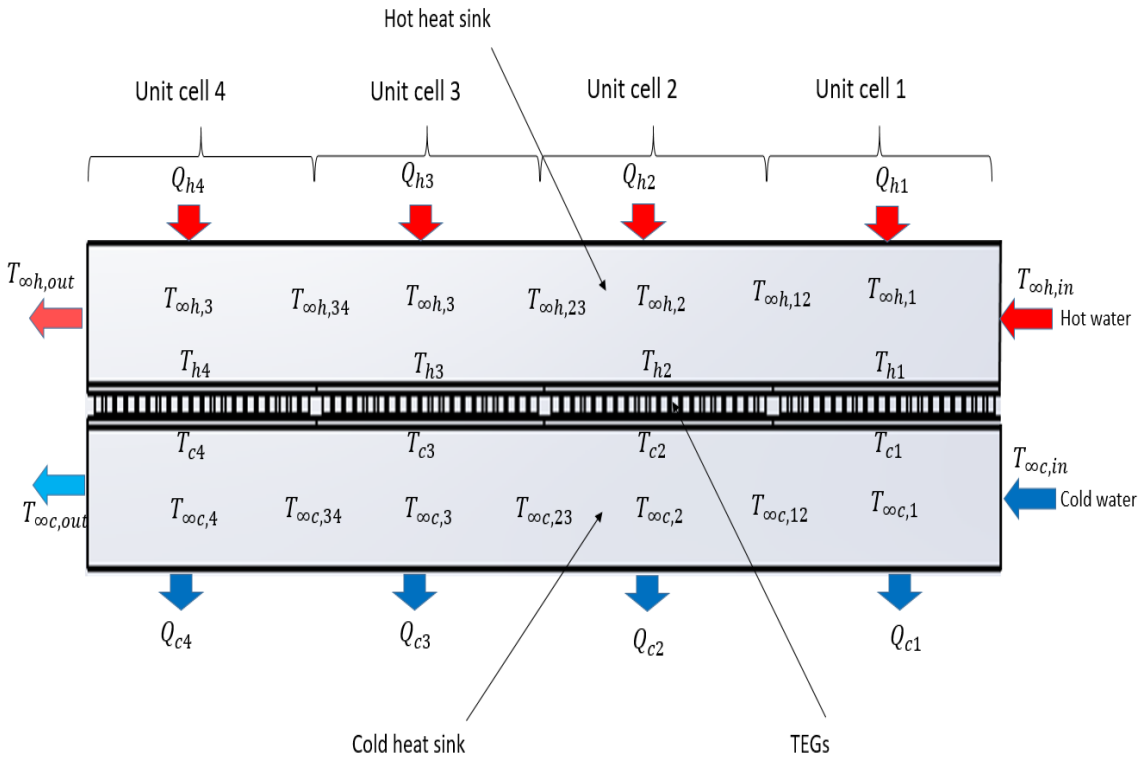

Figure 3.3 Schematic of the four unit cells system

The module properties, external loads, specific heats, mass flow rates and both inlet water temperatures ($T_{\infty h,in}$ & $T_{\infty c,in}$) are given where both hot and cold convection conductance parameters ($\eta_{s,h}h_hA_{s,h}$ & $\eta_{s,c}h_cA_{s,c}$) are calculated from the geometry of the heat sinks. The equations (equation 3.48 to equation 3.53) are converted into four non-dimensional equations around each unit cell where sixteen non-dimensional equations are the result of modeling the whole system as in the following.

$$N_h\left[\frac{1}{2}T^*_{\infty h,(i-1)i}+\frac{1}{2}T^*_{\infty h,i(i+1)}-T^*_{hi}\right] = N_{ki}\left[\left(\frac{T^*_{hi}-T^*_{ci}}{(R_{ri}+1)}\right)T^*_{hi}ZT_{\infty c,in}-\frac{(T^*_{hi}-T^*_{ci})^2}{2(R_{ri}+1)^2}ZT_{\infty c,in} + (T^*_{hi}-T^*_{ci})\right] \quad (3.57)$$

$$N_h\left[\frac{1}{2}T^*_{\infty h,(i-1)i}+\frac{1}{2}T^*_{\infty h,i(i+1)}-T^*_{hi}\right] = \beta_1\left[T^*_{\infty h,(i-1)i}-T^*_{\infty h,i(i+1)}\right] \quad (3.58)$$

$$N_h\left[T^*_{ci}-\frac{1}{2}T^*_{\infty c,i(i+1)}-\frac{1}{2}T^*_{\infty c,(i-1)i}\right] = N_{ki}\left[\left(\frac{T^*_{hi}-T^*_{ci}}{(R_{ri}+1)}\right)T^*_{ci}ZT_{\infty c,in}+\frac{(T^*_{hi}-T^*_{ci})^2}{2(R_{ri}+1)^2}ZT_{\infty c,in} + (T^*_{hi}-T^*_{ci})\right] \quad (3.59)$$

$$N_h\left[T^*_{ci}-\frac{1}{2}T^*_{\infty c,i(i+1)}-\frac{1}{2}T^*_{\infty c,(i-1)i}\right] = \beta_2\left[T^*_{\infty c,i(i+1)}-T^*_{\infty c,i(i+1)}\right] \quad (3.60)$$

The dimensionless temperatures are defined by

$$T^*_{hi}=\frac{T_{hi}}{T_{\infty c,in}} \quad (3.61)$$

$$T_{ci}^{*} = \frac{T_{ci}}{T_{\infty c,in}} \tag{3.62}$$

$$T_{\infty h,(i-1)i}^{*} = \frac{T_{\infty h,(i-1)i}}{T_{\infty c,in}} \tag{3.63}$$

$$T_{\infty c,(i-1)i}^{*} = \frac{T_{\infty c,(i-1)i}}{T_{\infty c,in}} \tag{3.64}$$

$$T_{\infty h,i(i+1)}^{*} = \frac{T_{\infty h,i(i+1)}}{T_{\infty c,in}} \tag{3.65}$$

$$T_{\infty c,i(i+1)}^{*} = \frac{T_{\infty c,i(i+1)}}{T_{\infty c,in}} \tag{3.66}$$

So, the dimensionless junction and water temperatures are functions of eleven independent parameters, except when $T_{\infty h,(i-1)i}^{*} = T_{\infty h,01}^{*}$ or $T_{\infty c,(i-1)i}^{*} = T_{\infty c,01}^{*}$ because these two dimensionless temperatures are set to be given.

$$T_{\infty h,(i-1)i}^{*} = f(N_{k1}, N_{k2}, N_{k3,}\, N_{k4}, R_{r1}, R_{r2}, R_{r3}, R_{r4,} N_h, T_{\infty h,in}^{*}, ZT_{\infty c,in}) \tag{3.67}$$

$$T_{\infty c,(i-1)i}^{*} = f(N_{k1}, N_{k2}, N_{k3,}\, N_{k4}, R_{r1}, R_{r2}, R_{r3}, R_{r4,} N_h, T_{\infty h,in}^{*}, ZT_{\infty c,in}) \tag{3.68}$$

$$T_{\infty h,i(i+1)}^{*} = f(N_{k1}, N_{k2}, N_{k3,}\, N_{k4}, R_{r1}, R_{r2}, R_{r3}, R_{r4,} N_h, T_{\infty h,in}^{*}, ZT_{\infty c,in}) \tag{3.69}$$

$$T_{\infty c,i(i+1)}^{*} = f(N_{k1}, N_{k2}, N_{k3,}\, N_{k4}, R_{r1}, R_{r2}, R_{r3}, R_{r4,} N_h, T_{\infty h,in}^{*}, ZT_{\infty c,in}) \tag{3.70}$$

$$T_{hi}^{*} = f(N_{k1}, N_{k2}, N_{k3,}\, N_{k4}, R_{r1}, R_{r2}, R_{r3}, R_{r4,} N_h, T_{\infty h,in}^{*}, ZT_{\infty c,in}) \tag{3.71}$$

$$T_{c5}^{*} = f(N_{k1}, N_{k2}, N_{k3,}\, N_{k4}, R_{r1}, R_{r2}, R_{r3}, R_{r4,} N_h, T_{\infty h,in}^{*}, ZT_{\infty c,in}) \tag{3.72}$$

The unknown dimensionless temperatures (equation 3.61 to equation 3.66) are obtained from solving the sixteen non-dimensional equations (equation 3.57 to equation 3.60) where N_h, $T_{\infty h,in}^{*}$ and $ZT_{\infty c,in}$ are set to be inputs and N_{k1}, N_{k2}, N_{k3}, N_{k4}, N_{k5}, R_{r1}, R_{r2}, R_{r3} and R_{r4} are obtained from optimizing the single unit cell.

CHAPTER IV

EXPERIMENTAL WORK

The objective of this experiment is to verify the accuracy of modeling the whole system, discussed in the previous chapter. The current chapter is to clearly explain how the experiment is constructed and tested. An experimental model is built to test commercial TEGs for liquid to liquid low grade waste heat recovery.

4.1 Experimental Setup

The schematic diagram and the photograph of the thermoelectric power generation system based on liquid to liquid low grade waste heat recovery are shown in figures 4.1 (a) and 4.2. This system is designed to validate the way of analyzing the analytical model. The system mainly consists of four thermoelectric generator modules (TEGs), two heat sinks (for hot and cold water), and data acquisition system. TEGs are sandwiched between the two heat exchangers and arranged to be connected thermally in parallel and electrically in series.

Commercial modules, Kryotherm (TGM-199-1.4-0.8) with dimensions of 40mm × 40 mm (each), are employed in this work where each module has 199 couples of thermoelectric elements. The leg length and cross section area of the element are 0.8mm and 1.96 mm^2 respectively. Since the module properties are not supplied with the modules, the effective material properties are estimated based on the maximum parameters provided by the manufacturer.

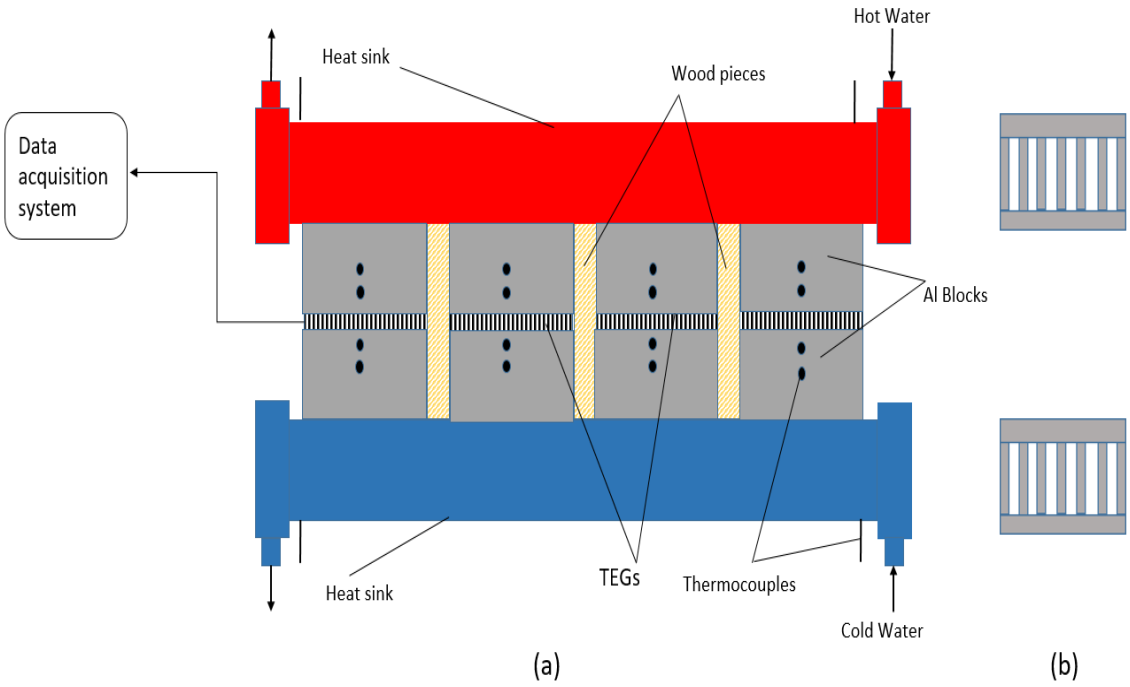

Figure 4.1 (a) Schematic of the experimental setup of four TEGs (b) Side views of the heat sinks

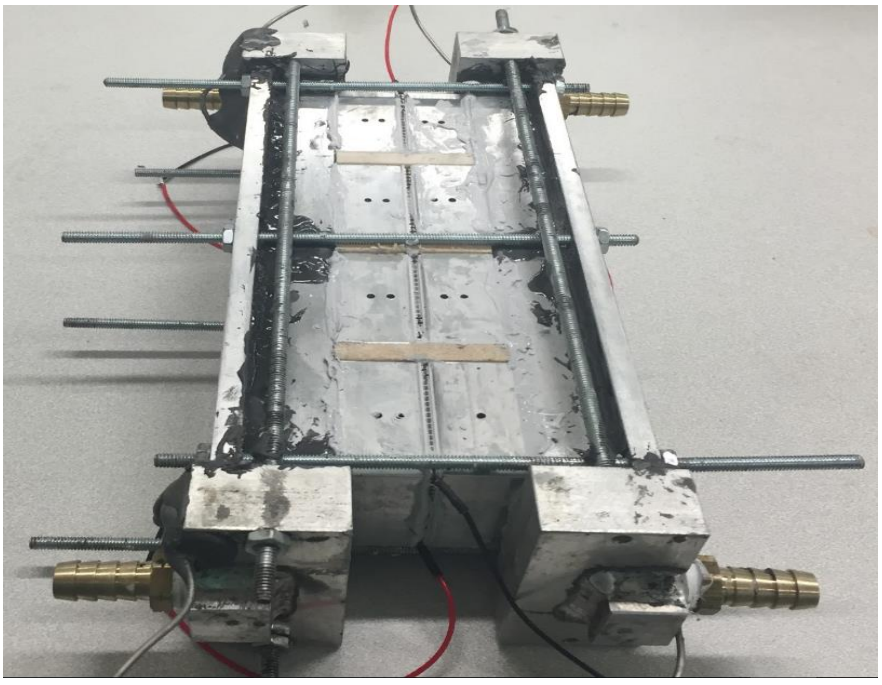

Figure 4.2 Photograph of the four TEGs system

Commercial aluminum heat sinks, with dimensions shown in table 4.1, are utilized to act as two plate-fin heat exchangers for the hot and cold water where two aluminum chambers are fixed at each end of the two heat sinks while two aluminum plates are placed on their upper surfaces. The chambers and plates, shown in figure 4.3 (a) & (b), are properly fabricated to be fit with the heat sinks to prevent water leakage.

Table 4.1 Commercial heat sink dimensions

Fin profile length (mm)	16.6
Fin thickness (mm)	2.3
Spacing (mm)	3.4
Width (mm)	40
Length (mm)	196
Height (mm)	20
Base thickness (mm)	3.6

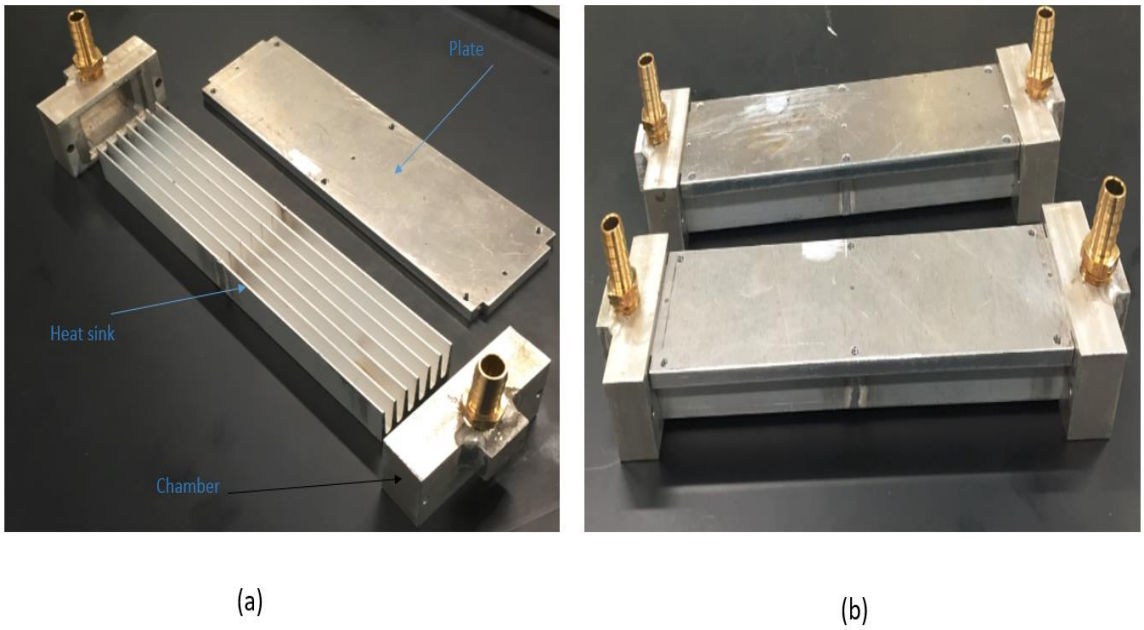

Figure 4.3 (a) Heat sink assembling (b) hot and cold heat sinks as plate-fin heat exchangers

Eight aluminum blocks (40mm×40mm×19.1mm of each) are fabricated to be sandwiched between each TEG module and its heat sink where each block has two holes as shown in figures 4.1 (a) and 4.2. The holes with a depth of 20 mm are made to be places for the thermocouples. Twenty thermocouples, K type, are used in this experiment where four for the inlet and outlet water temperatures along the heat sinks and the other for the junction temperatures. Three low thermal conductivity wood pieces (6mm× 19.1mm × 40mm of each) are inserted between the unit cells to minimize the conduction losses between each two of the aluminum blocks. The reason of using the aluminum blocks is to measure the junction temperatures along the block because it is experimentally difficult to measure the module junction temperatures directly.

Assuming linear change of temperature along the aluminum blocks, the two measured temperatures of each block can be extrapolated to obtain the junction temperature

($T_h$or T_c) of each module. The 6 Pass Heat Exchanger Demonstrator, shown in figure 4.4, is used in this work to provide the hot and cold water to the system where there are two flow meters to set the flow rates. Furthermore, the TEG system is insulated using a thermal insulator to reduce heat losses with environment as shown in figure 4.5.

Figure 4.6 shows the flow chart of the experimental setup. The experiment is conducted to measure the inlet and outlet water temperatures for both the heat sinks, the junction temperatures across the blocks, the generated current and the voltage at each module where Lab view program was created to control the readings. The measurements were taken by changing external load resistance seven times.

Figure 4.4 Photograph of the 6 Pass Heat Exchanger Demonstrator

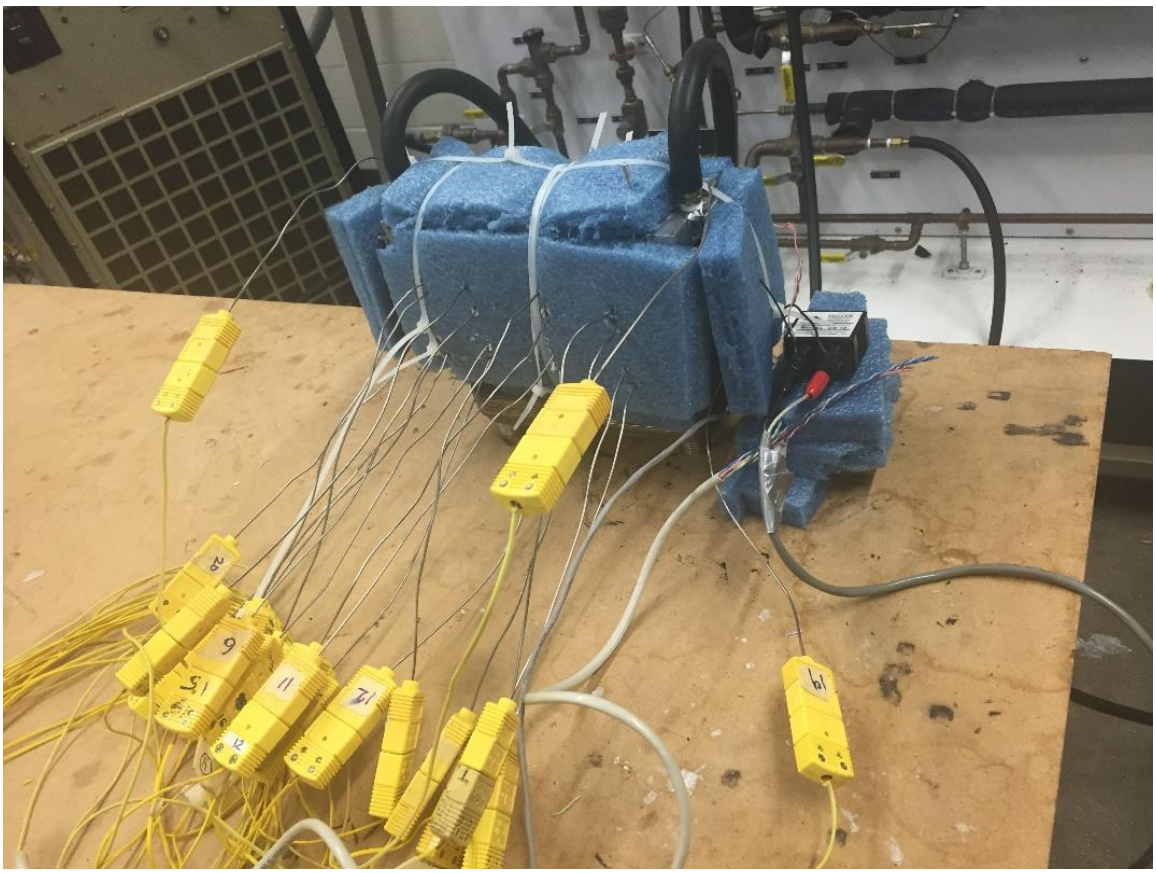

Figure 4.5 The TEG system with thermal insulation

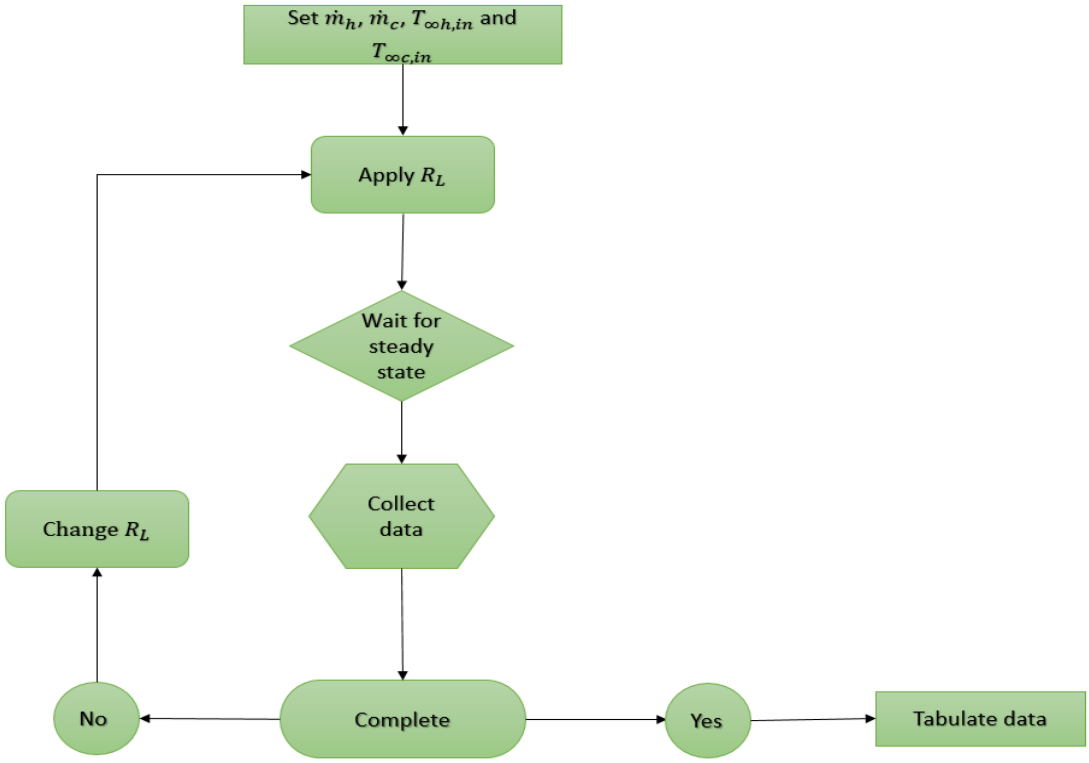

Figure 4.6 Flow chart of the experimental setup

4.2 Thermal Resistance of Aluminum Block

The overall heat sink efficiency was discussed in the previous chapter. In order to estimate the efficiency of heat sink with aluminum (η_s), the thermal resistance of the aluminum blocks must be considered [4]. The total thermal resistance (R_t) of heat sink with aluminum is defined by

$$\sum R_t = R_{t,s} + R_{t,al} \tag{4.1}$$

Which is expressed as

$$\frac{1}{\eta_s h A_s} = \frac{1}{\eta_o h A_s} + \frac{t_{al}}{k_{al} A_{al}} \tag{4.2}$$

Modifying equation 4.2, the heat sink efficiency is

$$\eta_s = \left(\frac{1}{\eta_o} + \frac{hA_s t_{al}}{k_{al} A_{al}}\right)^{-1} \tag{4.3}$$

Where η_o, h, A_s, t_{al}, k_{al} and A_{al} are heat sink overall efficiency, convection heat transfer coefficient, heat transfer area of heat sink, the thickness of the aluminum block, aluminum block thermal conductivity and conduction heat transfer area of aluminum block.

4.3 Obtaining Junction Temperatures of TEG Module

As mentioned in the experiment setup section, junction temperature (T_h or T_c) is obtained by extrapolating the two measured temperatures of its aluminum block. Figure 4.7 shows the schematic diagram of a unit cell with its aluminum blocks. The hot and cold junction temperatures are calculated as follows

$$T_h = 2T_{h1} - T_{h2} \tag{4.4}$$

$$T_c = 2T_{c1} - T_{c2} \tag{4.5}$$

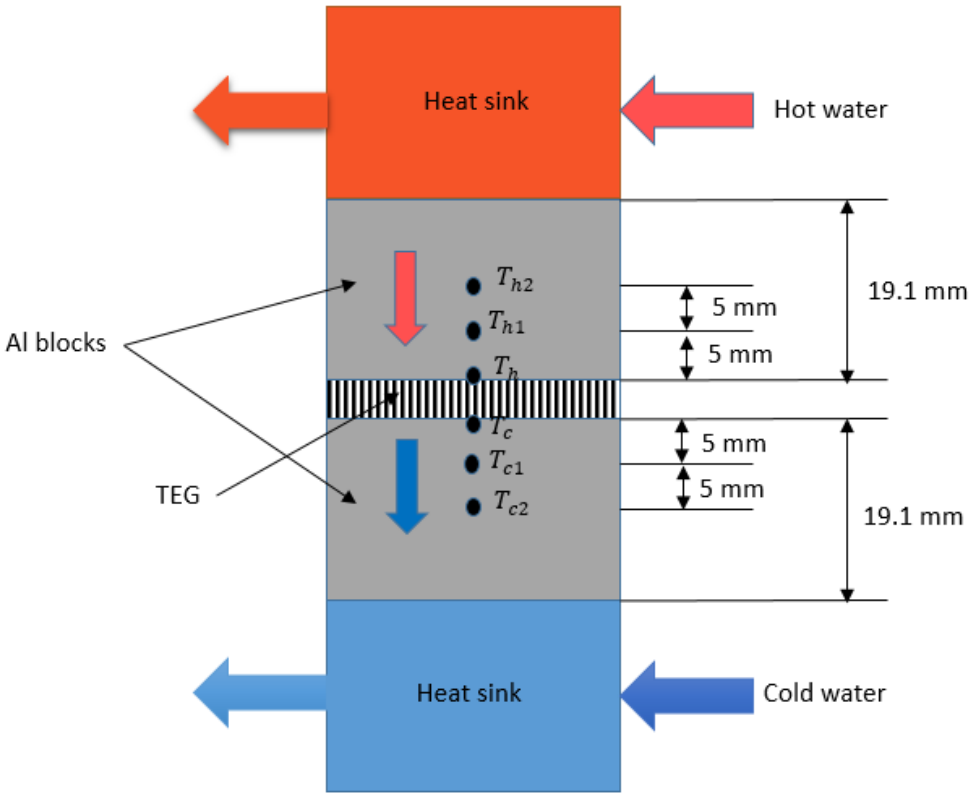

Figure 4.7 Schematic diagram of a unit cell with its aluminum blocks

CHAPTER V

RESULTS AND DISCUSSIONS

All information in this chapter is related to the methodologies discussed in chapters 3 and 4. The current chapter is to show and discuss all results in detail. The results of modeling and optimizing of the liquid-to-liquid unit cell for low grade waste heat recovery are introduced to identify its optimum design, where the optimal of the whole system is obtained based on these results. Two configurations, Parallel and counter flows, are considered in the whole system to display the difference. The effective material properties of the commercial module, used in the experiment, are obtained and validated with the manufacture performance curves. Furthermore, the experiential results of verifying the analytical model are presented.

5.1 Results of Liquid-to-Liquid Unit Cell Design

Modeling the unit cell, shown in figure 3.2 (a) & (b), for liquid-to-liquid low grade temperature requires to have hot and cold water inlet temperatures and hot and cold water flow as inputs. Heat sinks dimensions (both have the same), module properties and size are assumed as shown in table 5.1. Hot convection conductance ($\eta_{s,h}h_hA_{s,h}$) and cold convection conductance ($\eta_{s,c}h_cA_{s,c}$) are calculated from the equations of section 3.2. Then, junctions and outlet water temperatures are obtained from solving the six equations (equation 3.1 to equation 3.6). Power output and efficiency are plotted versus resistance ratio (R_r) as shown in figure 5.1. This figure shows that the maximum power output of

0.862 W is reached when $R_r = 1.2$ where the efficiency is 2%. For the given module and input conditions, the power output can be maximized by improving the heat transfer rate through the heat sinks.

Table 5.1 Assumed dimensions and inputs of the unit cell system

Heat sink dimensions ($A_b = 40mm \times 40mm$)	$b = 2\ cm$ $z = 4\ mm$ $t = 1.7\ mm$ $n = 7$
TEG properties ($40mm \times 40mm$) [4]	$\alpha = 3.256 \times 10^{-4} \frac{V}{K}$ $\rho = 2.048 \times 10^{-4} \Omega cm$ $k = 0.030 \frac{W}{cm\ K}$ $A_e = 1.96\ mm^2$ $L_e = 2mm$
Inputs and conditions	$T_{\infty h,in} = 90℃$ $T_{\infty C,in} = 20℃$ $\dot{V}_h = 3\ gpm$ $\dot{V}_c = 3\ gpm$

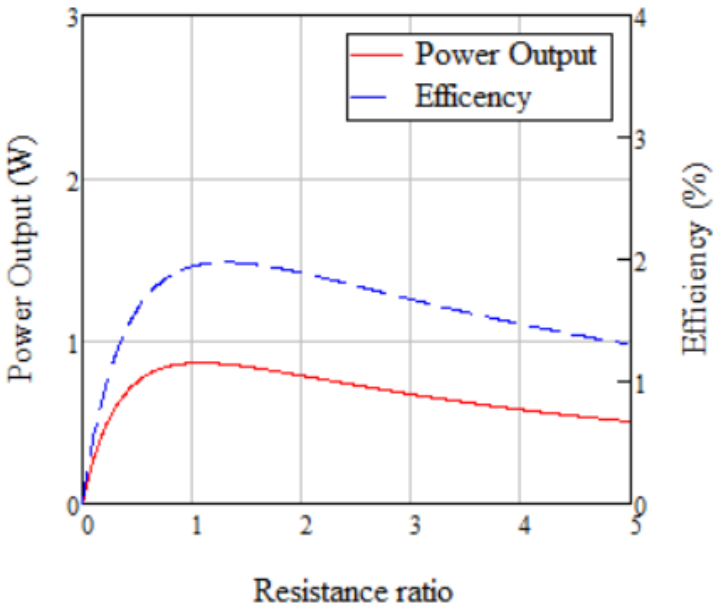

Figure 5.1 Power output and efficiency versus resistance ratio of the unit cell without optimization

5.2 Heat Sinks Optimization

To improve the heat transfer of the hot and cold sides of the unit cell, both convection conductance parameters ($\eta_{s,h}h_hA_{s,h}$ & $\eta_{s,c}h_cA_{s,c}$) should be maximized. The three parameters, profile length (b), spacing (z) and fin thickness (t) at a given base area ($A_b = 40mm \times 40mm$) can be optimized by plotting each convection conductance versus one parameter and fixing the other two at each time. Figure 5.2 shows the results of convection conductance versus fin profile length for (a) hot heat sink and (b) cold heat sink. From these two plots, the profile length is as small as the convection conductance is high. However, too small of a profile length would not be practical, so a profile length of 1cm instead of 2 cm is chosen for both heat sinks. A step appears in the figure 5.2 (a) and (b) because at profile length of 6.75cm in the hot side and 2cm in cold side the flow changes from turbulent into laminar. That is why these curves are not continuous.

Convection conductance parameters of both heat sinks are plotted versus spacing in figure 5.3 and versus fin thickness in figure 5.4. These two figures show that higher values of $\eta_{s,h}h_hA_{s,h}$ or $\eta_{s,c}h_cA_{s,c}$ are obtained when the spacing is smaller and fin thickness is larger. Even though choosing spacing of 2 mm and fin thickness of 2 mm is not the optimal, they are proper and reasonable values to use in the new design of both heat sinks. When the fin spacing of the cold side heat sink, shown in figure 5.3 (b), is 4.3 mm or more while the profile length and thickness are fixed, the flow is turbulent. Also, the flow becomes turbulent when the fin thickness of the cold side is 1.9 mm or more while the fin profile length and spacing are fixed as shown in figure 5.4 (b). Because of the change in flow from laminar into turbulent, these curves have steps. Table 5.2 shows a comparison of parameters for the heat sinks between the commercial (old design) and the optimized (new design).

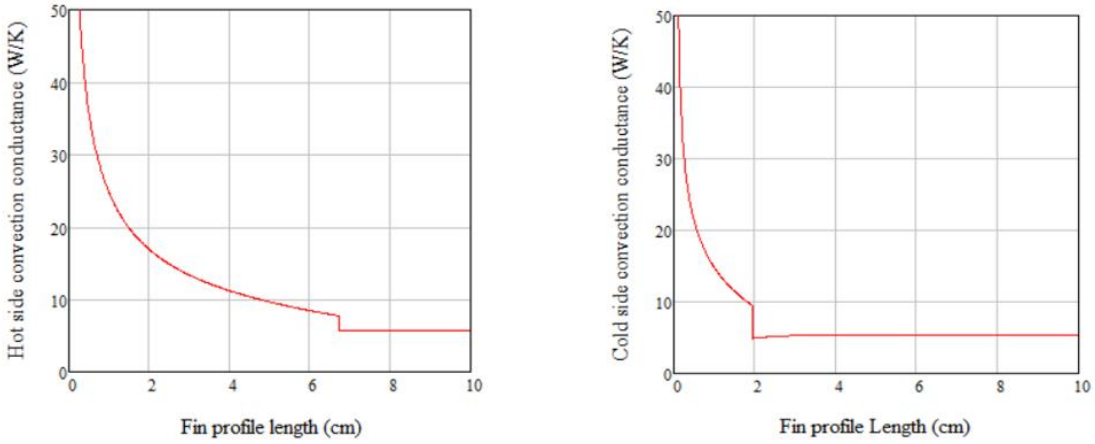

Figure 5.2 Convection conductance versus profile length (a) hot heat sink, (b) cold heat sink

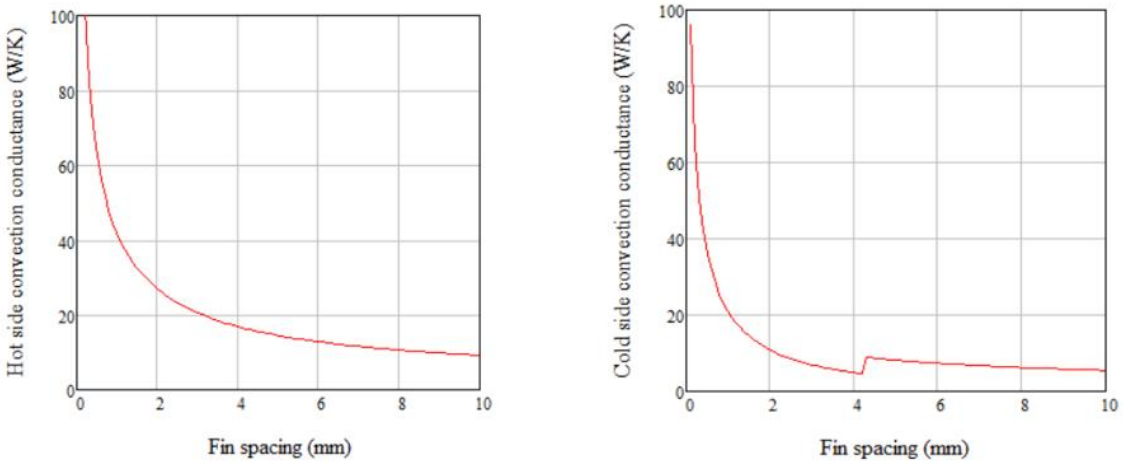

Figure 5.3 Convection conductance versus fin spacing (a) hot heat sink, (b) cold heat sink

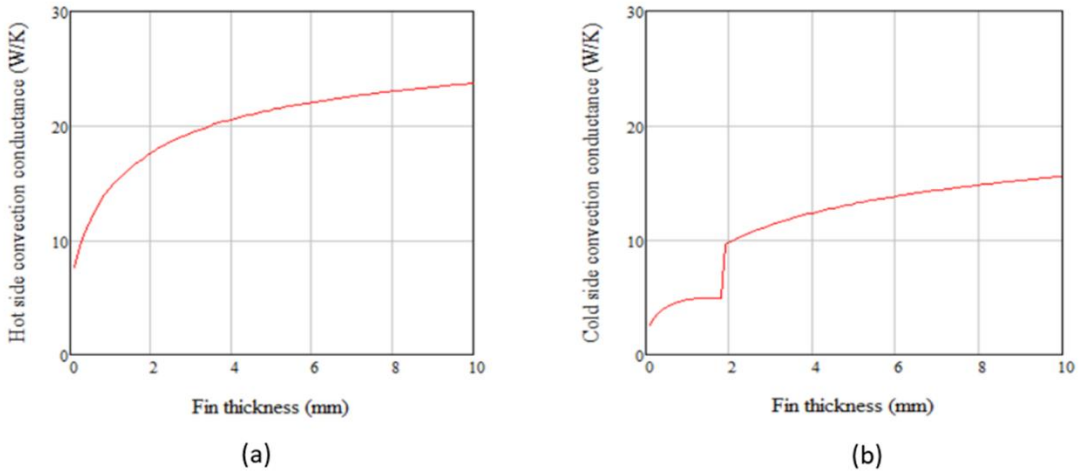

Figure 5.4 Convection conductance versus fin thickness (a) hot heat sink, (b) cold heat sink

Table 5.2 Comparison of parameters for the heat sinks between the old and new design

Parameter	Commercial (old design)		Optimized (new design)	
	Hot heat sink	Cold heat sink	Hot heat sink	Cold heat sink
Profile length, b	$2\ cm$	$2\ cm$	$1\ cm$	$1\ cm$
Spacing, z	$4mm$	$4mm$	$2mm$	$2\ mm$
Thickness, t	$1.7\ mm$	$1.7\ mm$	$2\ mm$	$2\ mm$
Number of fins, n	7	7	10	10
Convection heat transfer coefficient	$3453\ \frac{W}{m^2K}$	$537.3\ \frac{W}{m^2K}$	$9366\ \frac{W}{m^2K}$	$4260\ \frac{W}{m^2K}$
Total heat transfer area	$0.013\ m^2$	$0.013\ m^2$	$9.2 \times 10^{-3} m^2$	$9.2 \times 10^{-3} m^2$
Overall heat sink efficiency	0.381	0.715	0.467	0.615
Hot side convection conductance $\eta_{s,\mathrm{h}}\mathrm{h}_\mathrm{h}A_{s,\mathrm{h}}$	$16.887\ \frac{W}{K}$		$40.278\ \frac{W}{K}$	
Cold side convection conductance $\eta_{s,c}\mathrm{h}_c A_{s,c}$		$4.931\ \frac{W}{K}$		$24.121\ \frac{W}{K}$
Mass flow rate	$0.183\ \frac{kg}{s}$	$0.189\ \frac{kg}{s}$	$0.183\ \frac{kg}{s}$	$0.189\ \frac{kg}{s}$
Inlet water temperature	90 ℃	20 ℃	90 ℃	20 ℃

5.3 Liquid-to-Liquid Optimal Unit Cell Design

The optimum unit cell design is attained based on using the optimal method, discussed in section 3.3, that uses the non-dimensional parameters (N_k, R_r, T_h^*, T_c^*, $T_{\infty h,out}^*, T_{\infty h,out}^*, Q_h^*, Q_c^*$). These parameters can be obtained by solving equations 3.34 to 3.37 where N_h, $T_{\infty h,in}^*, ZT_{\infty c,in}$, β_1 and β_2 are set to be inputs. The new design of the hot and cold heat sinks is considered with the same input parameters used in section 5.1. Then, the performance of the unit cell is obtained for the given parameters. To find the optimum geometric ratio of the TEG and optimum resistance ratio, the two parameters, N_k and R_r, are optimized simultaneously. After that, the maximum power output can be obtained by using the optimum values of N_k and R_r.

Figure 5.5 shows power output, efficiency versus (a) dimensionless thermal conductance, N_k and (b) resistance ratio, R_r. The maximum power output of 6.165 W is obtained at optimum N_k of 0.488 and optimum R_r of 1.254 where the efficiency is 1.2%. It can be seen from this figure that the optimum N_k for maximum power output is different from the optimum N_k for maximum efficiency. While the optimum R_r for maximum power output is same as the optimum R_r for maximum efficiency. The efficiency can be increased from 1.2% to 1.6% by adjusting N_k to 0.3 instead of 0.484, which leads to an insignificant drop in power output as shown in figure 5.5 (a). However, the efficiency is still low, but it is not an important consideration in waste heat recovery system since heat is free. Therefore, power density (power output per TEG area) can be a good way to present a TEG performance. Power density is plotted versus dimensionless thermal conductance, N_k and versus resistance ratio, R_r as shown in figure 5.6 (a) and (b). It can be observed that from

N_k of 0.3 to 0.8, the power density has a small change, so choosing N_k of 0.3 does not affect either the power output or the power density and leads to increase the efficiency.

Power output and efficiency are plotted in figure 5.7 (a) versus geometric ratio and (b) versus leg length. This figure shows that when the geometric ratio is between 10 to 25, the power output changes a bit and it is close to the maximum. However, the efficiency drops as the geometric ratio increases. Therefore, the geometric ratio (G_e) of 12 would be good to use as an optimum value. In addition, the optimum leg length (L_e) is 0.16 mm where N_k is 0.3. It may be difficult to fabricate such leg length because it is complicated to measure the contact resistances.

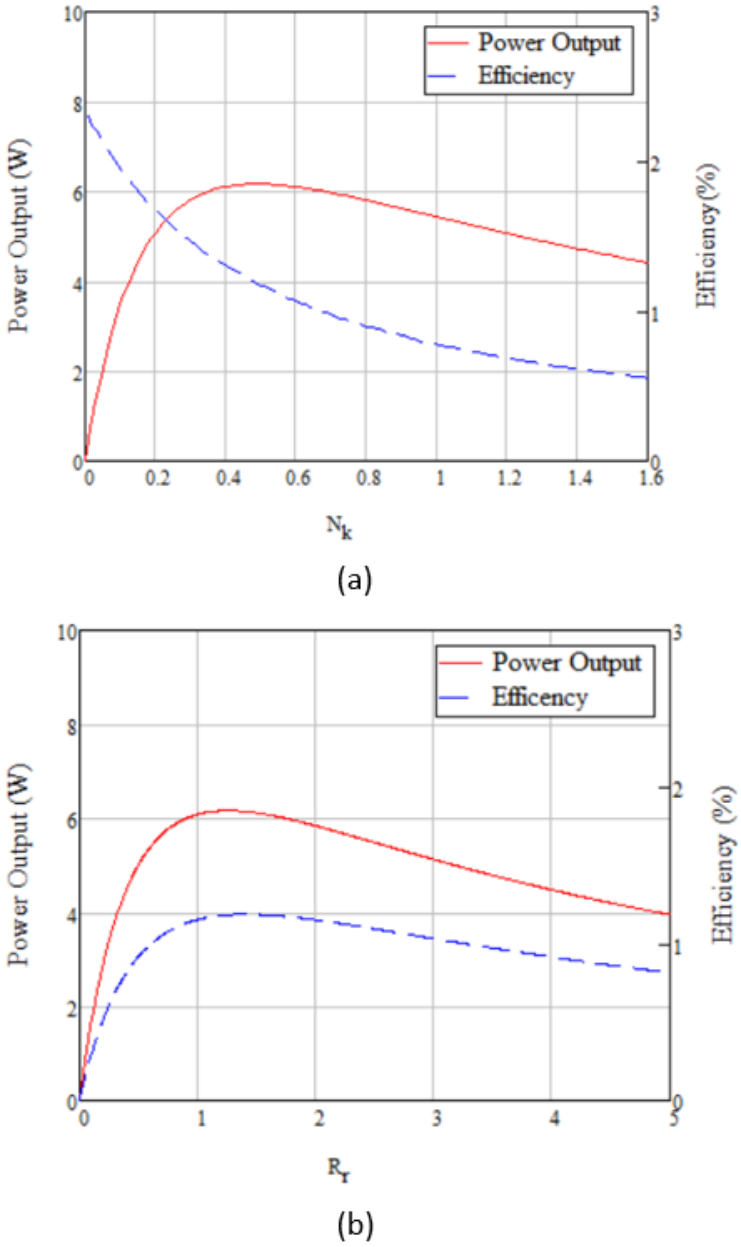

Figure 5.5 Power output, efficiency versus (a) dimensionless thermal conductance, $\boldsymbol{N_k}$, and (b) resistance ratio, $\boldsymbol{R_r}$, for the optimized unit cell

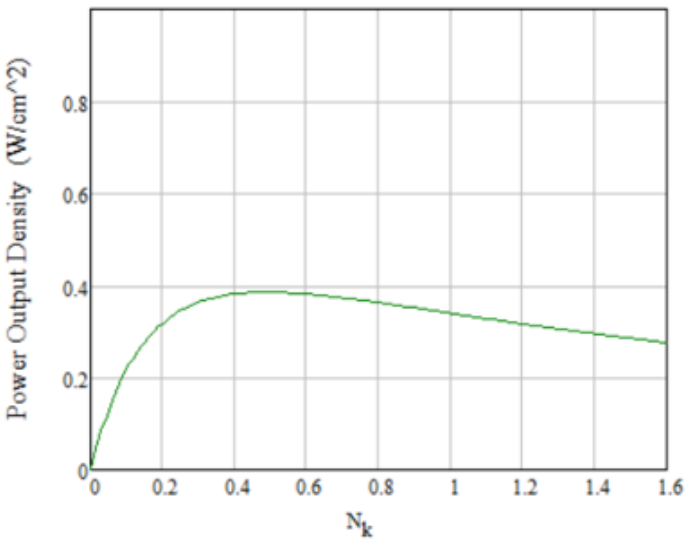

(a)

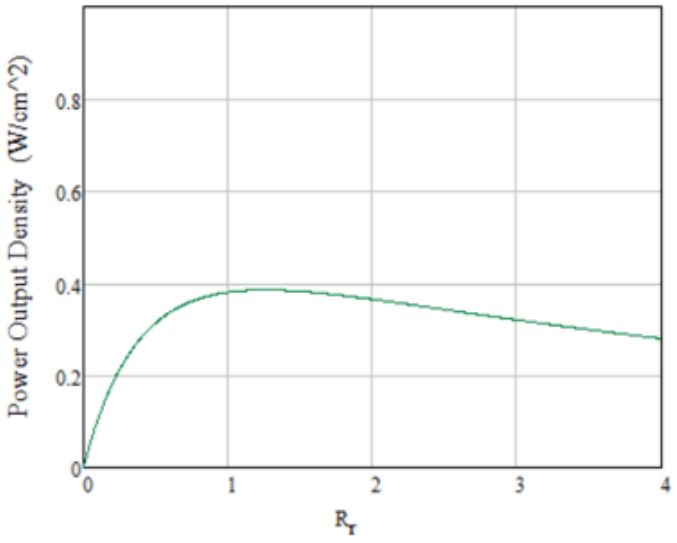

(b)

Figure 5.6 Power density versus (a) dimensionless thermal conductance, $\boldsymbol{N_k}$, and (b) resistance ratio, $\boldsymbol{R_r}$, for the optimized unit cell

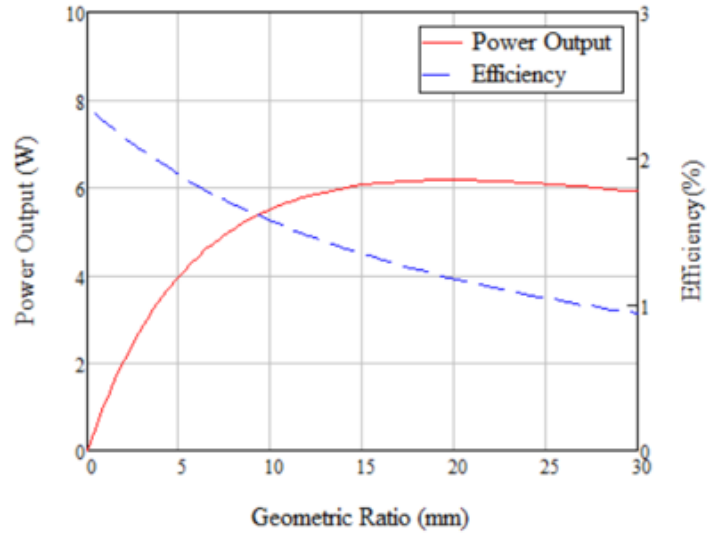

(a)

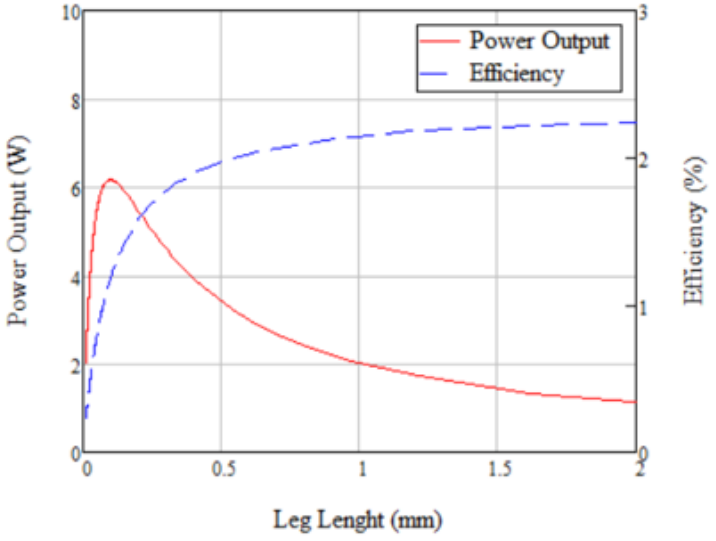

(b)

Figure 5.7 Power output, efficiency versus (a) geometric ratio and (b) leg length for the optimized unit cell

5.4 Optimal Design for The Four Unit Cells System

As mentioned, the whole system, shown schematically in figure 3.3, is divided into four isolated unit cells where each unit cell has one TEG. The geometry of the whole

system and the input parameters are shown in table 5.3. The results of the optimal design for the whole system are predicted based on the optimum N_k of 0.3 and optimum R_r of 1.254 of liquid-to-liquid optimal unit cell design, discussed in the previous section. Each dimensionless thermal conductance(N_{k1}, N_{k2}, N_{k3} and N_{k4}) is set to be equal to 0.3 and each resistance ratio (R_{r1}, R_{r2}, R_{r3} and R_{r4}) is set to be equal to1.254. N_h, $T^*_{\infty h,in}$ and $ZT_{\infty c,in}$ are inputs. Then, junction and water temperatures are calculated. After that, power output and efficiency are plotted versus N_k and R_r for each unit cell as shown in figure 5.8. It can be seen from this figure that the performance of each unit cell is more likely to be similar to each other. Also, all unit cells have the same optimum N_k and the same optimum R_r. The total power output and efficiency are plotted versus $N_k$and R_r for the whole system. The whole system produces about 22.3 W with efficiency of 1.4%, shown in figure 5.9, where the power density is about 0.36 at the optimum $N_k$and R_r. From this point, it can be concluded that optimizing one unit cell is enough to predict the optimal design for the whole system.

Table 5.3 Geometry of the heat sinks and input parameters for the four unit cells system

Heat sink dimensions (hot and cold sides) ($A_b = 40mm \times 160\ mm$)	$b = 1\ cm$
	$z = 2\ mm$
	$t = 2\ mm$
	$n = 10$
Inputs	$T_{\infty h,in} = 90℃$
	$T_{\infty C,in} = 20℃$
	$\dot{V}_h = 3\ gpm$
	$\dot{V}_c = 3\ gpm$

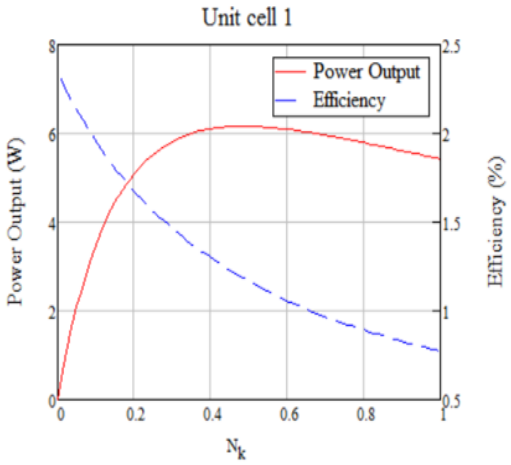
Unit cell 1
Power Output
Efficiency
Power Output (W)
Efficiency (%)
N_k

(a)

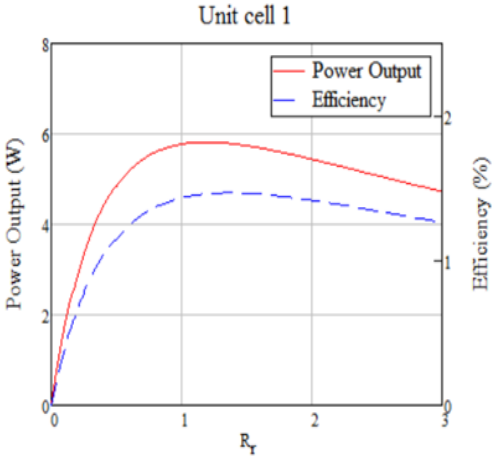
Unit cell 1
Power Output
Efficiency
Power Output (W)
Efficiency (%)
R_T

(b)

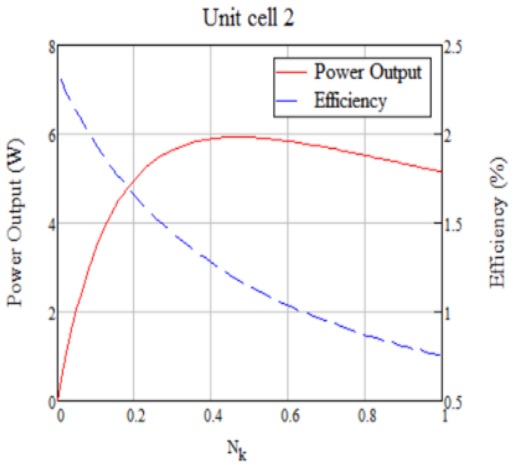
Unit cell 2
Power Output
Efficiency
Power Output (W)
Efficiency (%)
N_k

(c)

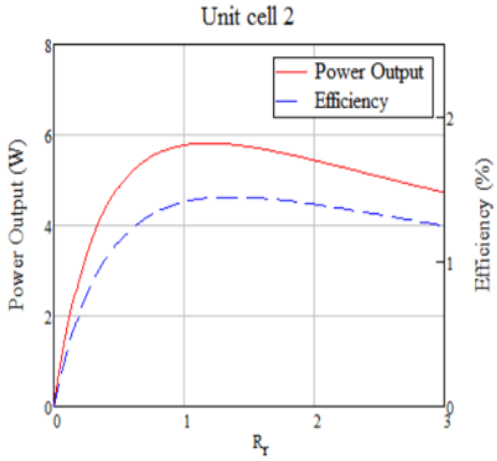
Unit cell 2
Power Output
Efficiency
Power Output (W)
Efficiency (%)
R_T

(d)

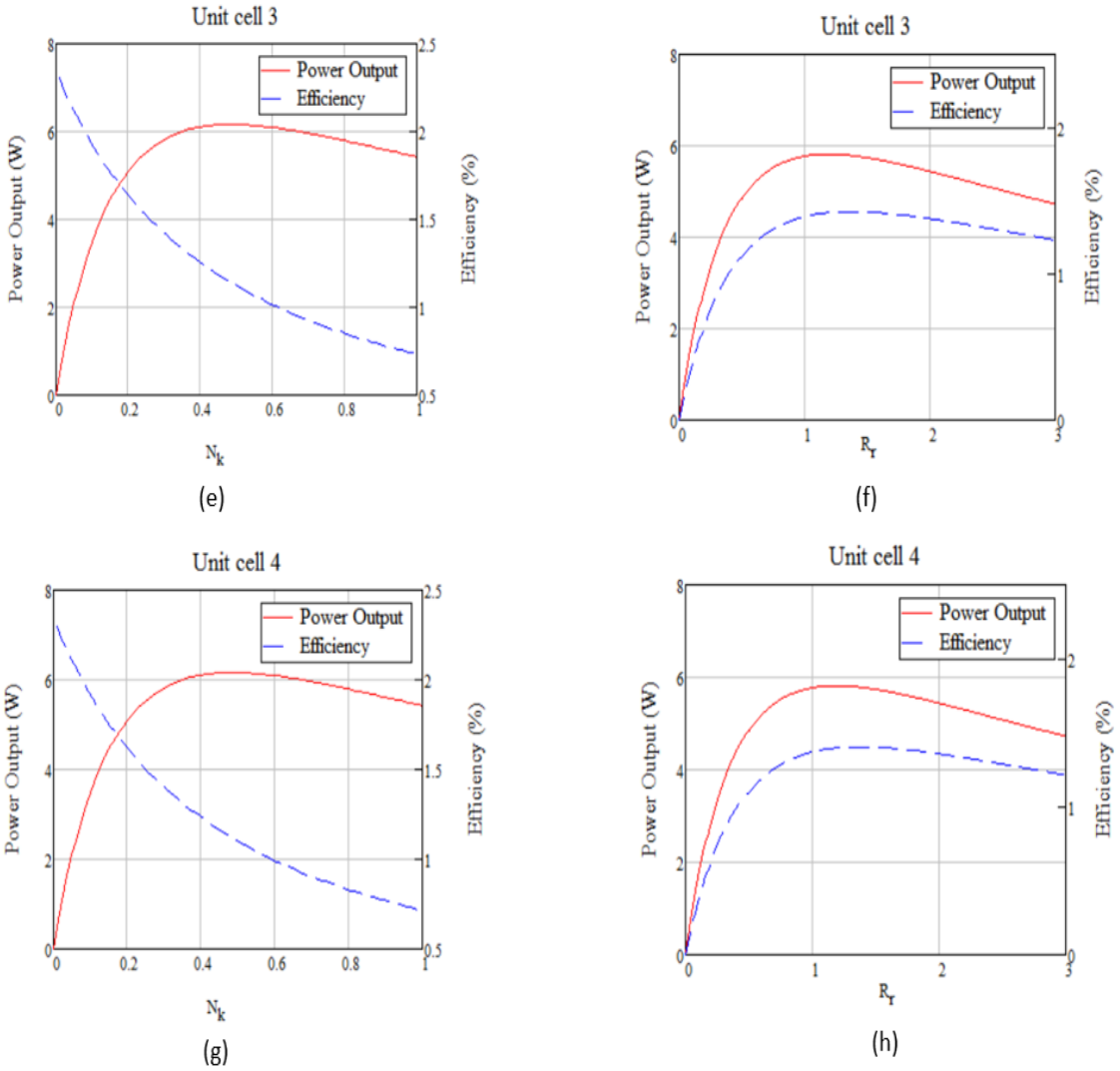

Figure 5.8 Power output and efficiency vs. thermal conductance, $\boldsymbol{N_k}$ and resistance ratio $\boldsymbol{R_r}$ for unit cell 1 (a, b), unit cell 2 (c, d), unit cell 3 (e, f) and unit cell 4 (g, h)

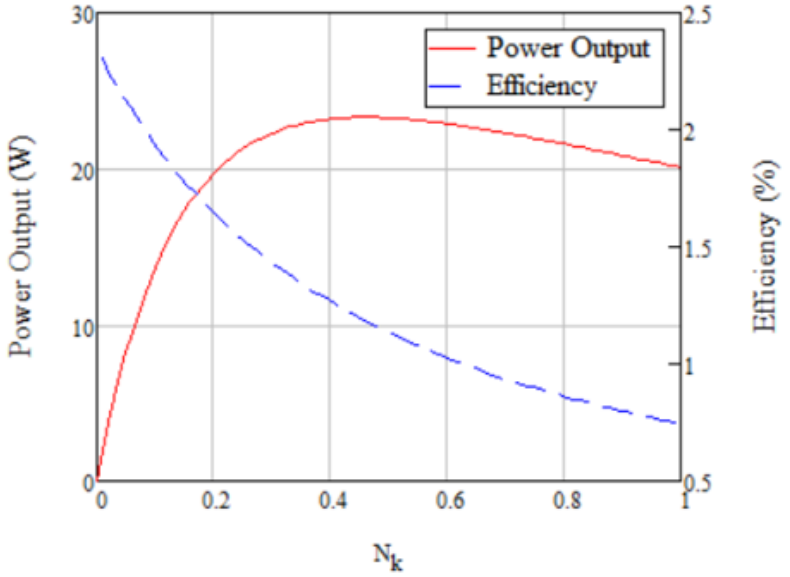

(a)

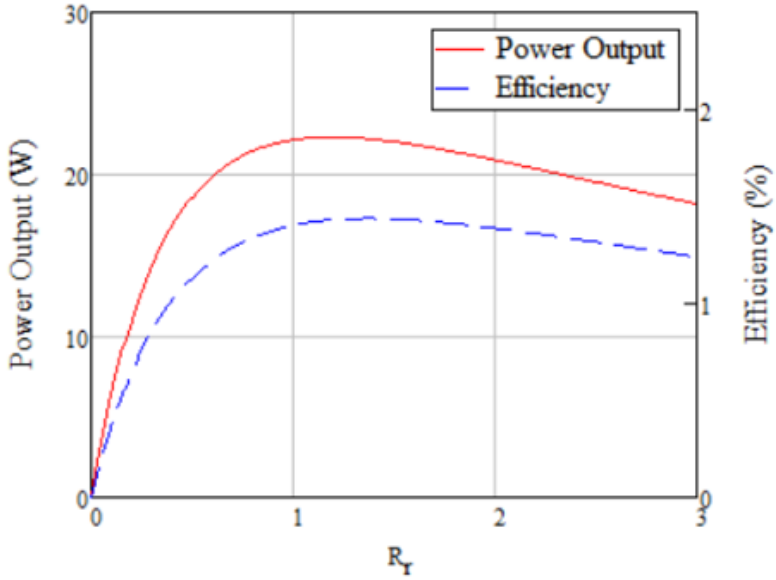

(b)

Figure 5.9 The total power output and total efficiency of the whole system vs. (a) thermal conductance, $\boldsymbol{N_k}$ and (b) resistance ratio $\boldsymbol{R_r}$

5.5 Comparison Between Parallel and Counter Flows

The results of the previous section were conducted by considering parallel flow for the system. This section is to compare two cases of flow, parallel and counter, to see the difference and figure out which one is more effective. Same system dimensions and same inputs are used in both cases.

Figure 5.10 shows junction temperatures of the four unit cells system and are plotted versus its position along the system in two cases where (a) parallel flow and (b) counter flow. It can be seen from this figure that the two plots (a &b) are almost similar because the difference in junction temperatures is small. Also, fluid temperatures (hot and cold water) are plotted versus the position as shown in figure 5.11. It can be observed that there is also a small difference between the two plots (a & b) of figure 5.11. However, there is a small convergence between both lines of the hot and cold water temperatures in the parallel flow while there is no convergence between the two lines in counter flow.

The difference between the parallel and counter flow can be seen in figure 5.12 where junction temperature difference is plotted versus the position in (a) parallel flow and (b) counter flow. In the parallel flow, the junction temperature difference (ΔT) drops along the system where the highest ΔT occurs at the first unit cell and lowest ΔT at the forth unit cell. However, ΔT seems to be constant along the system in the counter flow. Because the whole is considered as a small size, there is an insignificant difference in the performance of the system between the two flows. Since the counter flow can attain constant ΔT, it might be good to use with a large-scale system. The results of comparison between parallel and counter flow are illustrated in table 5.4.

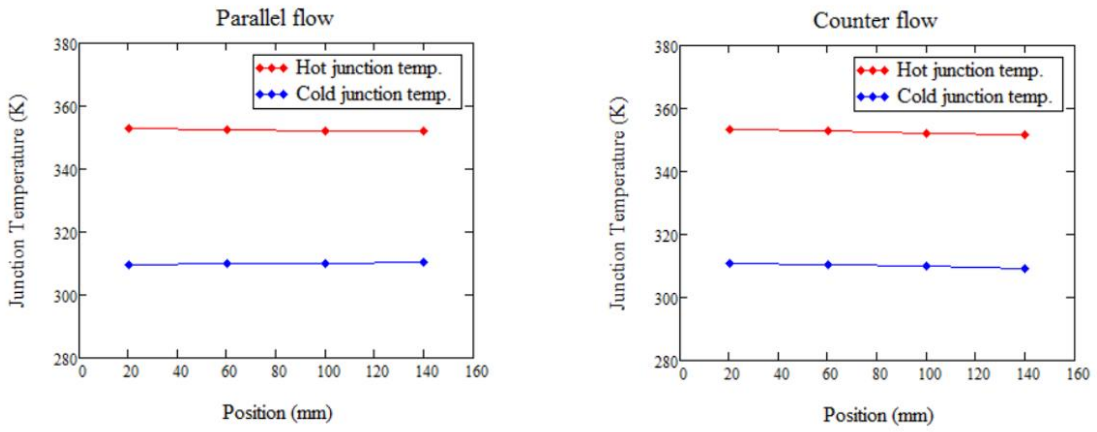

(a) (b)

Figure 5.10 Junction temperatures versus position along the four unit cells system for (a) parallel flow and (b) counter flow

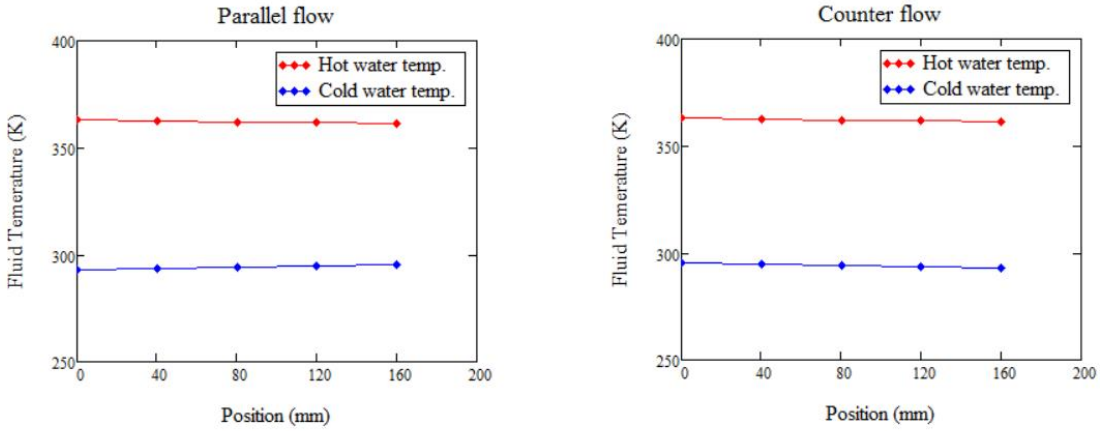

(a) (b)

Figure 5.11 Fluid temperatures versus position along the four unit cells system for (a) parallel flow and (b) counter flow

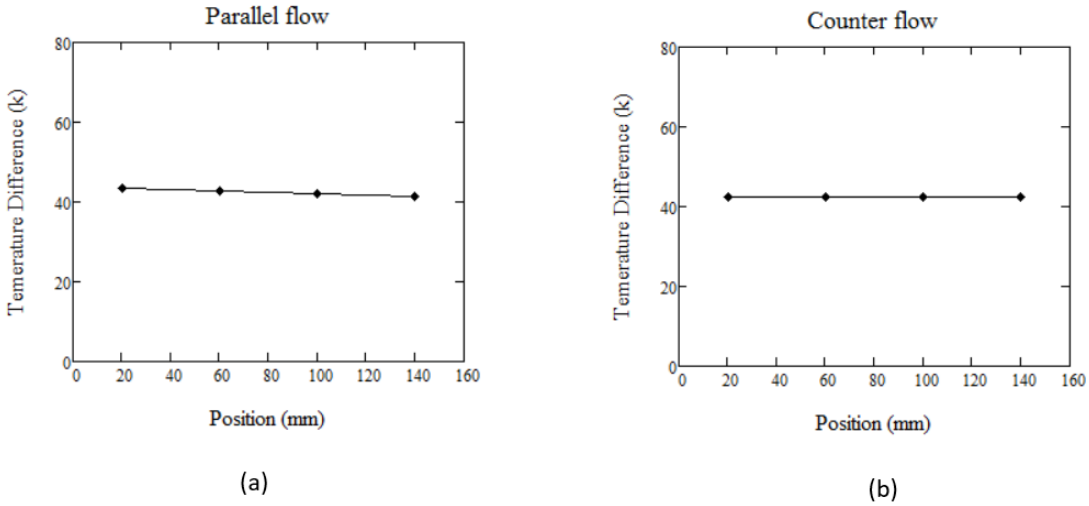

Figure 5.12 Junction temperature difference versus position along the four unit cells system for (a) parallel flow and (b) counter flow

Table 5.4 Comparison of results between parallel and counter flow for the optimal design of the four unit cells system

Parameter	Parallel flow	Counter flow
Total power output (W)	22.283	22.289
Efficiency (%)	1.4	1.4
Power density (W/cm^2)	0.348	0.348
Electric current (A)	0.678	0.664

5.6 Effective Material Properties

In order to validate the experimental model discussed in chapter 4 theoretically, the effective material properties of the commercial modules (TGM-199-1.4-0.8) used in the experiment are required. Using equations (equation 3.44 to equation 3.47) and based on the maximum parameters (I_{max}, V_{max} W_{max}, η_{max}) provided by the manufacturer, the module effective properties are obtained as illustrated in table 5.5. Also, the performance curves are calculated using the obtained effective material properties to compare with

manufacturer curves as shown in figure 5.13 (a), (b) and (c). The results are in good agreement with the manufacturer performance curves.

Table 5.5 Effective material properties for TGM-199-0.8-1.4

Description	Symbol (unit)	Value at $T_c = 30℃$
Provided maximum parameters	$I_{max}\ (A)$	5.6
	$V_{max}(\ V)$	8.2
	$W_{max}(\ W)$	11.4
	$\eta_{mp}(\%)$	4.1
	$R\ (\Omega)$	1.46
Geometry of thermoelements	L_e(mm)	0.8
	A_e(mm^2)	1.96
	n	199
Dimensions (W× L×H)	mm	40×40×3.2
Calculated effective material properties	α^*(V/K)	2.407×10^{-4}
	ρ^*(Ωcm)	$1.79\times10^{--3}$
	k^*(W/cmK)	0.027
	ZT_{av}	0.473
Calculated maximum parameters	$I_{max}\ (A)$	5.6
	$V_{max}(\ V)$	8.143
	$W_{max}(\ W)$	11.4
	$\eta_{mp}(\%)$	4.1
	$R\ (\Omega)$	1.454

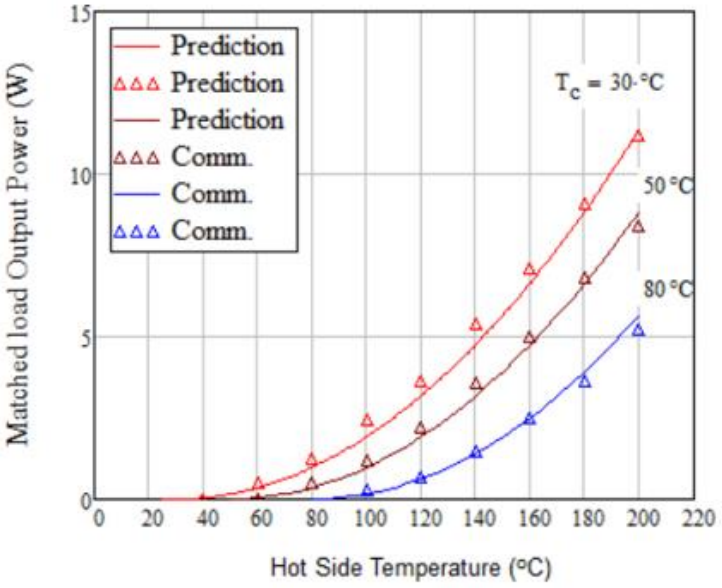
Prediction
Prediction
Prediction
Comm.
Comm.
Comm.
T_c = 30 °C
50 °C
80 °C
Matched load Output Power (W)
Hot Side Temperature (°C)
0
5
10
15
0
20
40
60
80
100
120
140
160
180
200
220

(a)

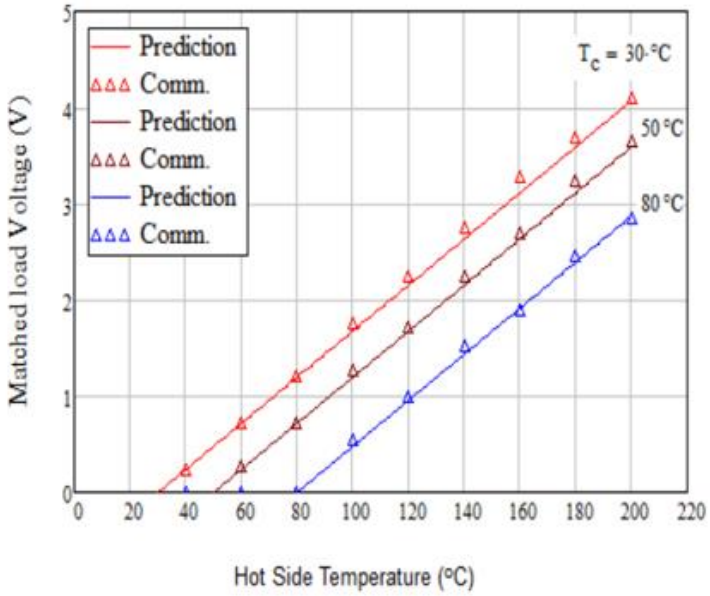
Prediction
Comm.
Prediction
Comm.
Prediction
Comm.
T_c = 30 °C
50 °C
80 °C
Matched load Voltage (V)
Hot Side Temperature (°C)
0
1
2
3
4
5
0
20
40
60
80
100
120
140
160
180
200
220

(b)

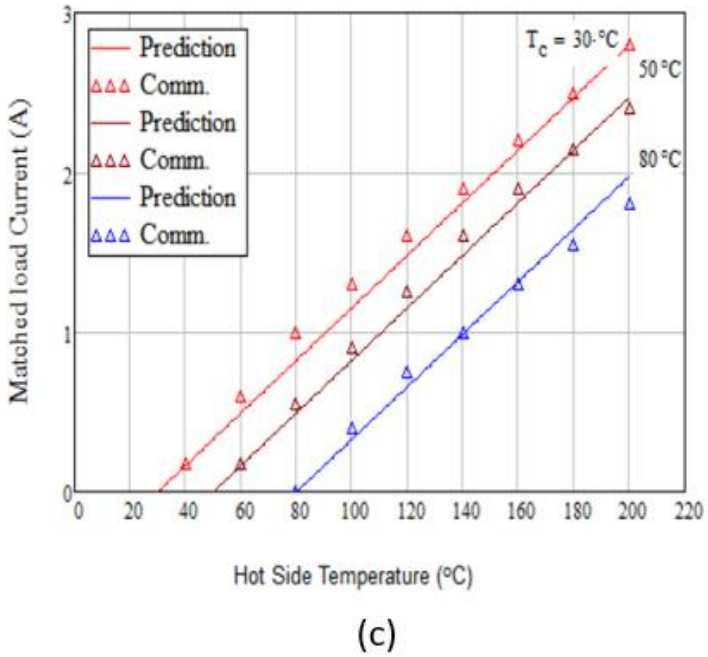

(c)

Figure 5.13 (a) Matched load output power, (b) matched load voltage and (c) matched load current vs. hot side temperature. For TEG-199-0.8-1.4, comparison between the obtained effective material properties with manufacturer performance curves

5.7 Experimental Model Validation

The experiment is conducted to check the accuracy of modeling the four unit cells for liquid to liquid low grade waste heat recovery. The analytical model of the four unit cells, discussed in section 3.5, is modified based on the experiment inputs, illustrated in table 5.6. This model consists of aluminum blocks, commercial heat sinks and commercial TEGs. The modified model is designed to compare with the experimental model. The measurements are obtained by considering two cases of flow, parallel and counter, as shown in figures 5.14 and 5.15 where the junction temperatures are plotted versus the resistance ratio. It can be seen from these two figures that the results of the parallel flow and counter flow are similar. The predicted and measured hot junction temperatures in the unit cell numbers 1, 3 and 4 are in good agreement while a small error appears in the unit

cell number 2 for both cases. Also, small discrepancies can be seen between the predicted and measured cold junction temperatures in all unit cells. These errors in the junction temperatures might be due to some heat losses with the environment. It might also be due to the assumption of temperature independent property. Using the effective material properties in the analytical model may be another cause of the errors.

The power output is plotted versus the resistance ratio in figure 5.16 to compare the results of the analytical model with the experimental model where (a) for parallel flow and (b) for counter flow. This figure shows that the predicted and measured power outputs are in good agreement in both parallel and counter flows. It can be observed from this figure that there is no significant difference between the two cases of flows. The measured power output is obtained from multiplying the measured current by the total measured voltage. Figure 5.17 shows the generated current versus the external load where (a) for parallel flow and (b) for counter flow. It can be seen from this figure that both cases of flow have similar results and there is a good agreement between the analytical and experimental results.

Figure 5.18 is plotted to compare the performance of the modified analytical model with and without aluminum blocks. It can be observed from this figure that thermal resistance of aluminum blocks drops the power output by about 28%. The reason for using the aluminum blocks was to measure the junction temperature, but there is no need for them in real system.

Table 5.6 Experimental input parameters

Description	Value
Hot water temperature	55.5℃
Cold water temperature	17.4℃
Hot water flow rate	1.9 gpm
Cold water flow rate	2.9 gpm

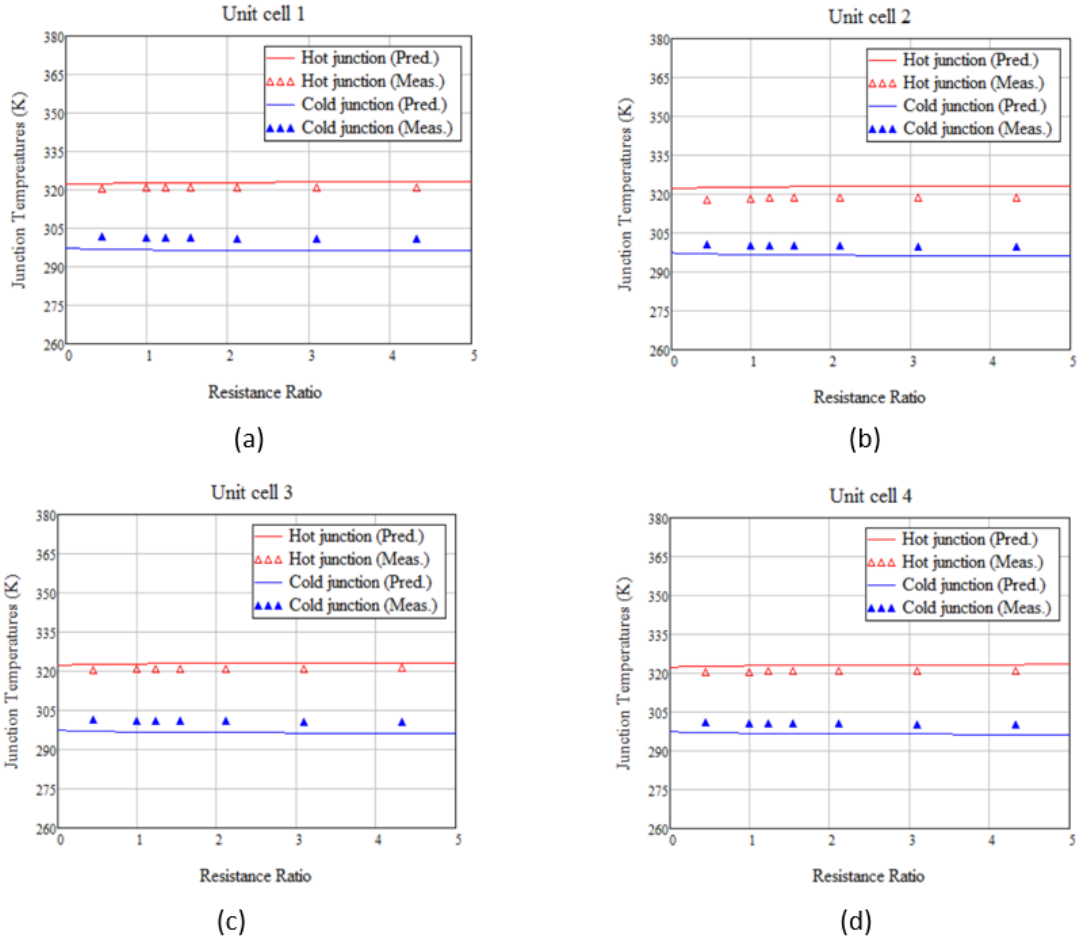

Figure 5.14 Junction temperatures versus resistance ratio of (a) unit cell 1, (b) unit cell 2, (c) unit cell 3 and (d) unit cell 4 for parallel flow

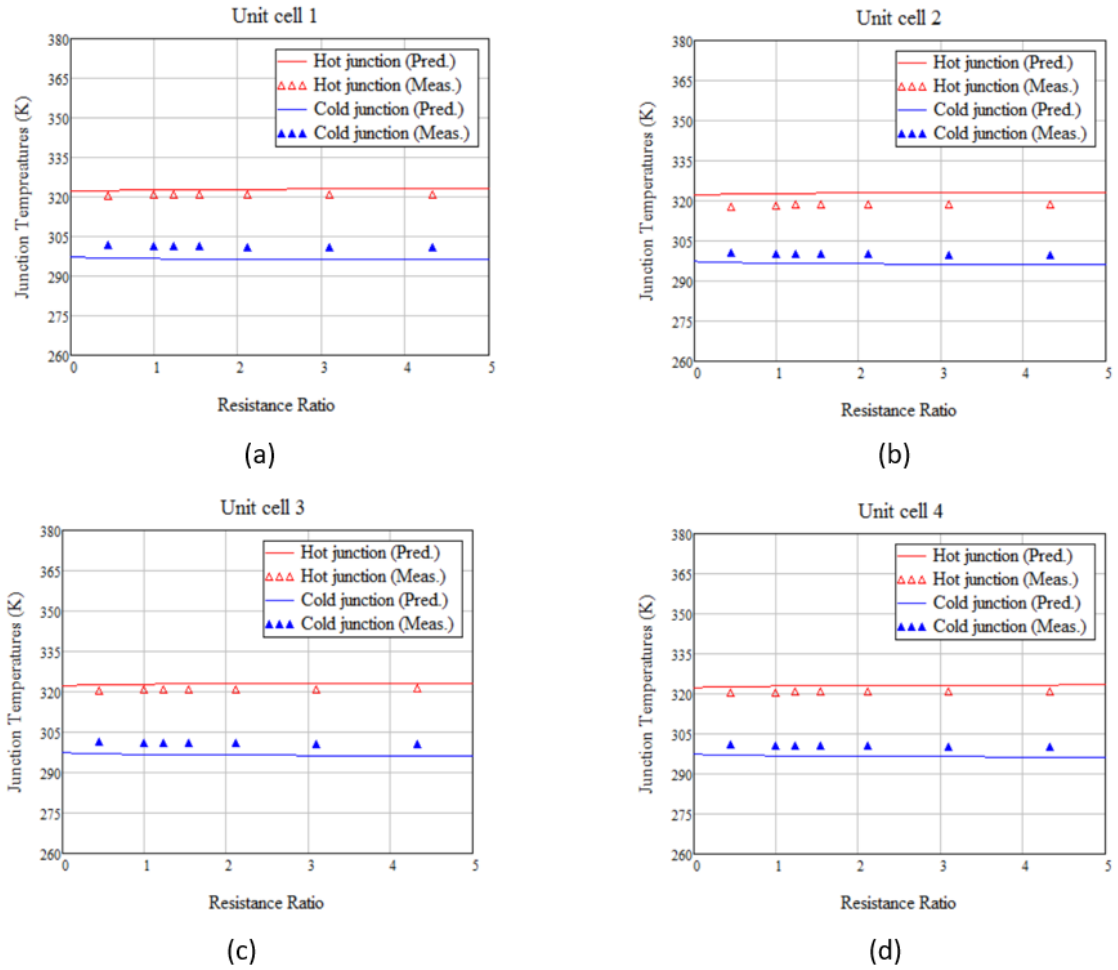

Figure 5.15 Junction temperatures versus resistance ratio of (a) unit cell 1, (b) unit cell 2, (c) unit cell 3 and (d) unit cell 4 for counter flow

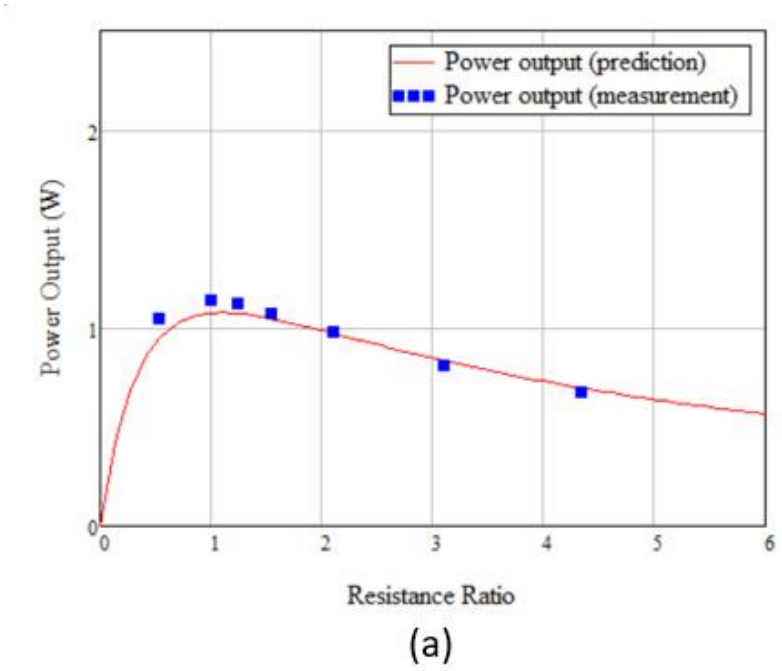

(a)

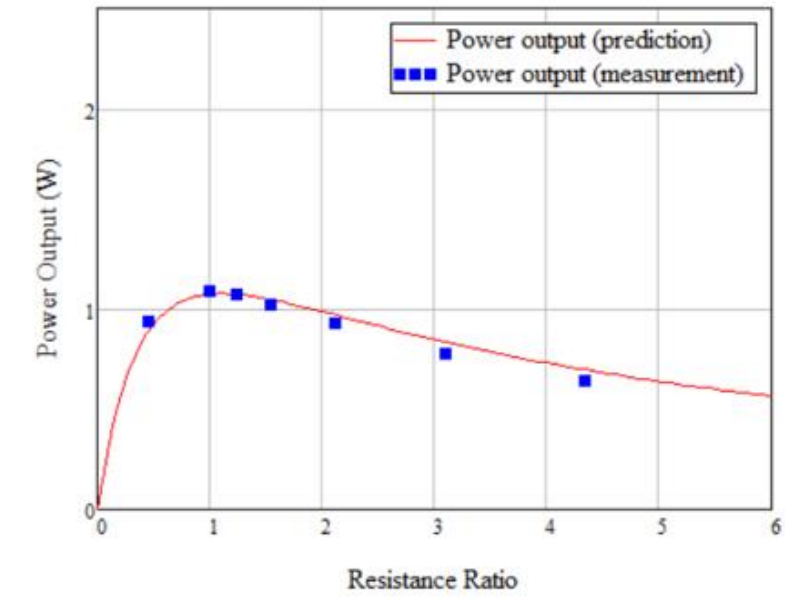

(b)

Figure 5.16 Comparison between the predicted and measured results of power outputs versus resistance ratio for (a) parallel flow and (b) counter flow

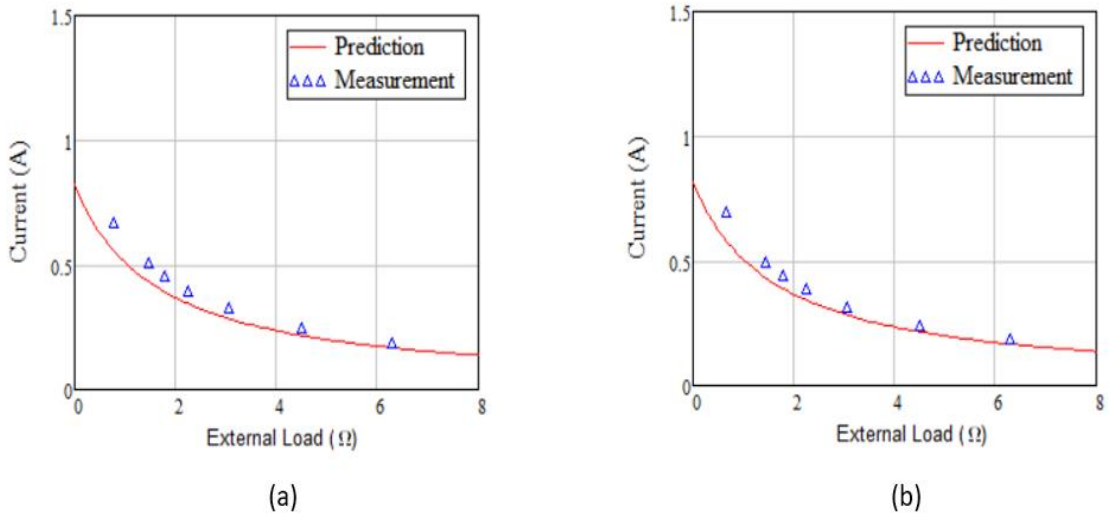

Figure 5.17 Comparison between predicted and measured current versus external load for (a) parallel flow and (b) counter flow

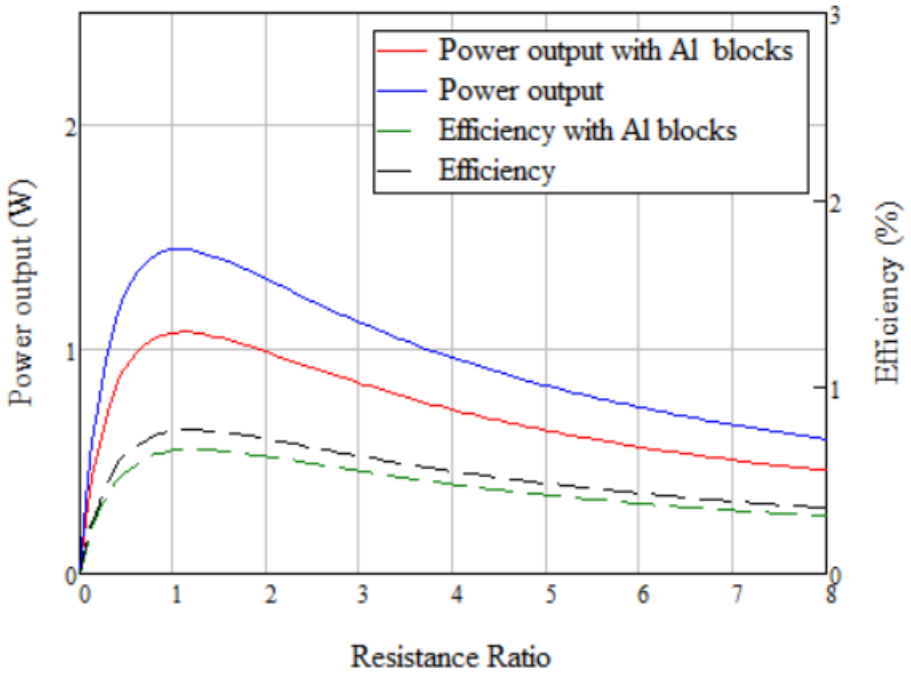

Figure 5.18 Comparison of power output and efficiency versus resistance ratio with and without aluminum blocks

CHAPTER VI

CONCLUSION

The main goal of this work was to study thermoelectric generators for liquid to liquid low grade waste heat recovery. A single unit cell of thermoelectric power generation was modeled based on the six heat equations and optimized by applying the non-dimensional method that allowed us to simultaneously optimize two parameters. The objective of optimization was to maximize the power output and the efficiency by finding the optimum element leg length of the TEG. The hot and cold heat sinks were also optimized to enhance the heat transfer on both sides of the unit cell. After obtaining an optimal design for the unit cell, a system of liquid-to-liquid four unit cells was simulated by combining the optimal design method with the thermal isolation method. The experiment, which used commercial TEGs module and heat sinks, was conducted to verify the way of modeling the four unit cells system by considering parallel and counter flows. The experimental results showed a good agreement between the analytical and experimental models although there were small discrepancies between the predicted and measured cold junction temperatures.

The feasibility of using thermoelectric generators for low grade waste heat was demonstrated in this work even though the optimal design of the four unit cells system was not validated experimentally. This was because the optimum element leg length of the TEG is not available commercially, so the optimal design can be demonstrated by fabricating such leg length. Also, the performance of thermoelectric generators can be improved for

low grade waste recovery by developing a specific heat exchanger for liquid to liquid heat transfer.

REFERENCES

[1] K. Ebrahimi, G. F. Jones and A. S. Fleischer, "A review of data center cooling technology, operating conditions and the corresponding low-grade waste heat recovery opportunities," *Renewable and Sustainable Energy Reviews,* vol. 31, pp. 622-638, 2014.

[2] K. Matsuda, "Low heat power generation system," *Applied Thermal Engineering,* vol. 70, no. 2, p. 1056, 05/2014.

[3] V. Minea, "Power generation with ORC machines using low-grade waste heat or renewable energy," *Applied Thermal Engineering,* vol. 69, no. 1-2, pp. 143 - 154, 08/2014.

[4] H. Lee, Thermoelectrics: Design and Materials, Hoboken, NJ: John Wiley & Sons, Inc, 2016.

[5] H. Lee, Thermal Design: Heat Sinks, Thermoelectrics, Heat Pipes, Compact Heat Exchangers, and Solar Cells, Hoboken, NJ: John Wiley & Sons, Inc, 2010.

[6] A. Attar, "Studying the Optimum Design of Automotive Thermoelectric Air Conditioning," Western Michigan University, Kalamazoo, 2015.

[7] L.-D. Zhao, V. P. Dravid and M. G. Kanatzidis, "The panoscopic approach to high performance thermoelectrics," *Energy& Environmental Science,* vol. 7, no. 1, pp. 251-268, 2014.

[8] M. D. Rowe, G. Min, S. G. K. Williams, A. Aoune, K. Matsuura, V. Kuznetsov and L. W. Fu, "Thetmoelectric recovery of waste heat-case studies," *Energy Conversion Engineering Conference,* pp. 1075-1079, 1997.

[9] D. T. Crane and G. S. Jackson, "Optimization of cross flow heat exchangers for thermoelectric waste heat recovery," *Energy Conversion and Management,* vol. 45, pp. 1565-1582, 2004.

[10] J. Yu and H. Zhao, "A numerical model for thermoelectric generator with the parallel- plate heat exchanger," *Jounral of Power Sources,* vol. 172, pp. 428-434, 2007.

[11] X. Niu, J. Yu and S. Wang, "Experimental study on low-temperature waste heat thermoelectric generator," *Journal of Power Sources,* vol. 188, pp. 621-626, 2009.

[12] X. Gou, H. Xiao and S. Yang, "Modeling, experimental study and optimization on low-temerature waste heat thermoelectric generator system," *Applied Energy*, vol. 87, pp. 3131-3136, 2010.

[13] D. Dai, Y. Zhou and J. Liu, "Liquid metal based thermoelctric generation system for waste heat recovery," *Renewable Energy*, vol. 36, pp. 3530-3536, 2011.

[14] X. Gou, S. Yang, H. Xiao and Q. Ou, "A dynamic model for thermoelectric generator applied in waste heat recovery," *Energy*, vol. 52, pp. 201-209, 2013.

[15] H. Lee, "Optimal design of thermoelectric devices with dimensional analysis," *Applied Energy*, vol. 106, pp. 79-88, 2013.

[16] A. Attar, H. Lee and S. Weera, "Experimental validation of the optimum design of an automotive air-to-air thermoelectric air conditioner (TEAC)," *Journal of ELECTRONIC MATERIALS*, vol. 44, no. 6, pp. 2177-2185, 2015.

[17] H. Lee, A. Attar and S. L. Weera, "Performance Prediction of Commericial Thermoelctric Cooler Modules using the Effective Material Properties," *Journal of ELECTRONIC MATERIALS*, vol. 44, pp. 2157-2165, 2015.

[18] A. Attar and H. Lee, "Designing and Testing the Optimum Design of Automotive Air-to-Air Thermoelectric Air Conditioner (TEAC) System," *Energy Conversion and Management*, vol. 112, pp. 328-336, 2016.

APPENDICES

A. Nomenclature

T_h Hot junction temperature (℃)

T_c Cold junction temperature (℃)

α Seebeck coefficient (V/K)

ρ Electrical resistivity $(\Omega\ cm)$

k Thermal conductivity $(\frac{W}{mK})$

Z The figure of merit $(\frac{1}{K})$

n The number of thermocouples

L_e Element leg length (mm)

A_e Element cross section area (mm^2)

G_e Element geometric ratio (mm)

R Electrical resistance (Ω)

K Thermal conductance $(\frac{W}{K})$

$\dot{m}$ Mass flow rate (kg/s)

c_p Specific heat ($\frac{J}{kg\ K}$)

T_∞ Fluid temperature (℃)

h Convection heat transfer coefficient ($\frac{W}{m^2\ K}$)

A_s Total heat transfer area of heat sink (mm^2)

I Electrical current (A)

R_L External load resistance (Ω)

b Fin profile length of heat sink (cm)

z Fin spacing of heat sink (mm)

t Fin thickness of heat sink (mm)

N_k Dimensionless thermal conductance

N_h Dimensionless convection

R_r Dimensionless electrical resistance

$\eta_{s,h} h_h A_{s,h}$ Hot side convection conductance ($\frac{W}{K}$)

$\eta_{s,c} h_c A_{s,c}$ Cold side convection conductance ($\frac{W}{K}$)

Subscripts

h Hot

c	cold
in	inlet
out	outlet
i	Unit cell number

B. Data Sheet of the Commercial Module

KRYOTHERM Company

6 Aerodromnaya street, Saint-Petersburg, 197348 Russia
Tel.: +7 (812) 394-1310 Fax: +7 (812) 394-1267 E-mail: info@kryotherm.ru
http://www.kryotherm.ru

SPECIFICATION

Thermoelectric Generating Module
Type TGM-199-1,4-0,8

Consumer parameters:

Parameter	tc=50.°C th=150.°C	tc=30.°C th=200.°C
U, V	2.50	4.10
I, A	1.75	2.80
P, W	4.30	11.40
Efficiency, %	2.60	4.10

1. tc - temperature of cold side;
2. th- temperature of hot side;
3. All parameters are given at module's internal resistance, equal to the resistance of the load.

Design parameters:

1. Electrical resistance (Rac at 22°C), Ohm - 0.95 ± 10%
2. Heat resistance, K/W - 0.57 ± 10%
3. Dimension, mm - 40,0x40,0/40,0x40,0 +0,5 / -0,2
4. Height, mm - 3.2 ± 0,050 ±0,025
5. Quantity, pcs - 20

Country of origin - Russia

Date: "03" июня 2006

Approved by quality control S.Zarubo

Thank you for your choice of KRYOTHERM product

KRYOTHERM
6 Aerodromnaya street, Saint-Petersburg, 197348 Russia
Tel: +7 812 394-13-10, fax: +7 812 394-12-67, E-mail: info@kryotherm.ru, http://www.kryothermtec.com

SPECIFICATION OF GENERATING THERMOELECTRIC MODULES TGM-199-1.4-0.8

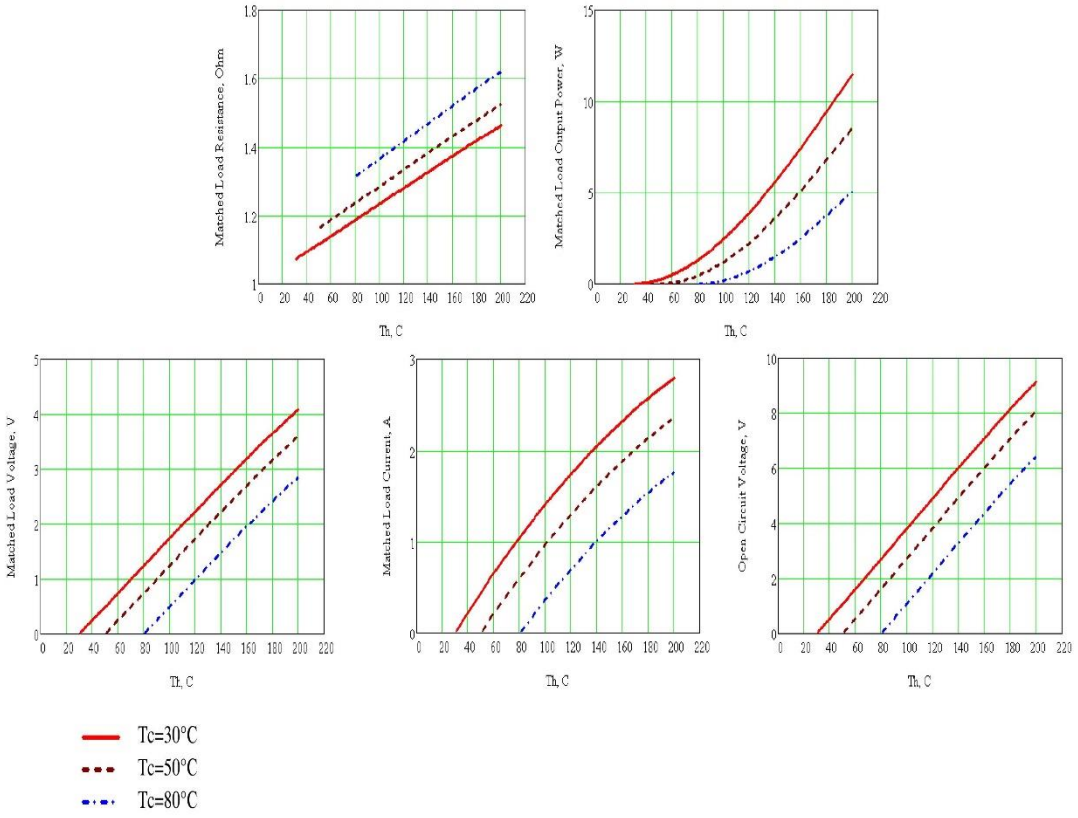

Kryotherm

Customer